SISSA ISAS
SCUOLA INTERNAZIONALE SUPERIORE DI STUDI AVANZATI
INTERNATIONAL SCHOOL FOR ADVANCED STUDIES

Spectral evolution of GRBs: new insights into their physics

Thesis submitted for the degree of
"Doctor Philosophiæ"

CANDIDATE

Giancarlo Ghirlanda

SUPERVISORS

Prof. Annalisa Celotti
Prof. Gabriele Ghisellini
Dr. Marco Tavani

October 2002

Dedicated to the memory of my mother

Contents

I would like to thank my supervisor, Annalisa Celotti, for her guiding and supporting me during these three years of PhD research. I am particularly grateful to Annalisa and Gabriele Ghisellini because they showed me how to approach in a positive, critical and open–minded way any scientific possibilities that one might encounter during the research process.

Many thanks also to Dr. David Band for his careful reading of this thesis and for his constructive comments on it.

I am also grateful to all my friends and colleagues and particularly to Roberta and Stefano who supported me in the final rush.

Introduction

Since their discovery in the late sixties, Gamma-ray Bursts (GRBs) have been one of the greatest puzzles of science. They are intense bursts of gamma ray photons with energy in the range 0.1-1 MeV lasting few tens of seconds, with heterogeneous spectral and temporal features. The progress in the knowledge of their observational characteristics and, consequently, of their theoretical interpretation, has always been strictly connected with the technological advances in the detectors and satellites design for the specific observation and study of these transient and extremely energetic events.

GRBs were discovered by the VELA satellites monitoring the respect of the nuclear test ban treaty (Klebesadel et al. [84]). Their existence was confirmed by the observations of the soviet Konus satellites (Mazets et al. [103]) and subsequently by other missions. The low positional accuracy of these first experiments did not allow for their distance determination and opened the first great debate about their energetics. In fact, if GRBs were placed at cosmological distances, their observed fluences, implied a huge ($E \leq 10^{54}$ erg) isotropic energy.

The distance problem was partially solved by the discovery of their isotropic distribution (Meegan et al [108]) by the Burst And Transient Source Experiment (BATSE) on board the Compton Gamma Ray Observatory (CGRO), launched in spring 1991. This detector, which accumulated a large homogeneous collection of GRBs (more than 3000) during its nine year activity, provided the first solid hint about their cosmological origin combining the evidence of an isotropic space distribution with a deficiency of faint GRBs with respect to a homogeneous distribution of sources in Euclidean space. BATSE also supplied additional informations on GRBs: their spectra were confirmed to have a non–thermal character (see chap.3 for details) typically represented by a single or multiple power law (Band et al. [4]) with a break in the energy range 200 - 300 keV. The light curves show single smooth peaks or complicated multipeaked structures, the burst durations range from 1 ms to about 1000 sec, with a bimodal distribution separated at ~ 2 sec (Kouveliotou et al. [86]), and an anticorrelation between the spectral hardness and duration, with the short bursts being harder than long ones (e.g. Fishman & Meegan [38]).

The cosmological origin of GRBs was definitely confirmed in 1997 by the observation of their counterparts by the Italian - Dutch satellite Beppo-SAX. The first X-ray afterglow discovery (GRB 970228 - Costa et al. [17]) was followed by an increasing number of afterglow observations (at a rate of about 10 yr^{-1}) at other wavelengths (e.g. van Paradijs et al. [124], Frail et al. [43]) which allowed the determination of the redshift and the study of the host galaxies (Kulkarni et al. [87]). The first redshift measurement, from the absorption line in the optical transient of GRB 970508, resulted in z=0.835 (Frail et al. [43]) and the actual redshift distribution for 20 GRBs (Djorgovsky et al. [30]) has a mean value $< z >= 1.27$ and extends to $z_{max} = 4.5$, for GRB 000131 (Andersen et al. [2]).

The host galaxies seemed to be faint galaxies with intense on–going star formation (Djorgovsky et al. [30], Totani et al. [155]): this evidence supports the massive star progenitor scenario (Woosley [162], Pazcynski [121], Vietri et al. [157]) in which the burst is expected to explode in the same region where its progenitor was formed, and has important cosmological implications for the study of the star formation rate (e.g. Lamb [89]).

The afterglow observations also provided some evidence of the possible anisotropic structure of GRBs, with an opening angle of about $\sim 5°$ (Israel et al. [73], Sari et al. [142], Frail et al. [44]), while the possible detections of iron lines in a few X–ray afterglows (Piro et al. [127]) have been interpreted to constrain environment densities and bursts energetic (Ghisellini et al. [58]).

The discovery and analysis of 17 X–Ray Flashes (XRF) detected by the Wide Field Camera (on board SAX) in the 2-26 keV energy range, with duration between 10 and 200 sec and quite isotropic sky distribution, have been recently reported by Heise et al. ([69]). The comparison of their temporal and spectral properties with classical GRBs seems to favor the idea that XRF could be the low energy (X–ray) extension of the GRB population (Kippen et al. [81]).

A possible theoretical interpretation of these observational evidences has been proposed through the "standard" fireball scenario. According to this model the inner engine of GRBs releases a large amount of energy ($\sim 10^52$ erg) in a small volume ($\sim 10^7$ cm) then producing a relativistic outflow which expands in the surrounding medium, i.e. the fireball. The energy and matter density is initially so high that these components thermalize and when the fireball becomes transparent it should release its internal energy in form of thermal photons. The typical non thermal character of GRB spectra, instead, motivated the formulation of an efficient mechanism for the extraction of the internal energy and then for its conversion into non thermal radiation. The simplest model of energy transport in the relativistic flow is in the form of kinetic energy of particles. A proposed variant is based on the possibility that a fraction of energy is transported by Poynting flux (Spruit et al. [151]). Among the possible mechanisms for the conversion of this energy into radiation, the most successful was the internal/external shock model. The internal shocks (Rees & Meszaros [133]), which are produced by the collision of fireballs with different Γ, accelerate the electrons responsible of the synchrotron emission. The external shock (Meszaros & Rees [112]) is determined by the deceleration of the fireballs by the ISM and produces the Afterglow emission.

Some observational confirms of this model have been found: the scintillation of the radio afterglow of GRB 970508 (Goodman et al. [62], Frail et al. [43]) and its optical spectrum, proved the small size of the emission region representing a "direct" measure of the relativistic expansion. Another important observational fact was the narrow range of peak energies of the bursts spectra, typically clustered around 300 keV which is predicted by synchrotron emission under particular assumptions. Finally the observations of the breaks in the afterglow light curves, if interpreted as due to the expansion of the jet (Sari et al. [144], Kulkarni et al. [87]), would require a beamed (anisotropic) fireball model (Rhoads [134], Sari et al. [144]).

Currently the most widely accepted scenarios for the progenitor of GRBs are the collapsar or single star model (Woosley [162], Paczynski [121], Fryer et al. [45]) or the merger of NS and/or BH in binary systems (Paczynski [119], Goodman [61], Meszaros & Rees [112]).

This thesis presents the time resolved spectral analysis of a sample of bright long bursts observed by BATSE and discusses the main findings in the light of the proposed emission models.

GRB spectra are characterized by several properties and by different evolution morphologies on small timescales (briefly reviewed in chapt.2). Extensive analysis of burst samples, with high spectral and temporal resolution (e.g. Preece et al. [130]) has led to the definition of these spectral properties. No unique spectral shape seems to describe all spectra which span a rather wide range of slopes at low and high energies. Moreover, no clear trends in the spectral evolution emerged from previous spectral analysis due to the large variety of evolutionary morphologies.

Within this observational picture we analyzed the time resolved spectra of bright bursts, on the smallest timescale available, in order to determine if there is a preferential function, among those typically assumed to represent the spectrum, which better fits the time resolved or time integrated spectra and in order to investigate the differences between the spectrum integrated on the duration of single pulses or time resolved within the same pulses.

The analysis of 25 bursts, with high temporal and spectral resolution BATSE data, is presented in chapter 5. The procedure adopted for the data reduction and their analysis is presented in chapter 4.

The most accepted scenario for the GRB prompt emission is synchrotron radiation of relativistic electrons in a strong magnetic field (Katz [77], Tavani [154]). This model predicts, in its simplest formulation, a limiting slope for the spectrum at low energies ($F(E) \propto E^{1/3}$) which agrees with different spectral evidences. Nonetheless, a considerable number of bursts (15%) was found to be harder than this limit.

An important test for the optically thin synchrotron model, which we performed for the first time on the time resolved spectra of bright bursts, is the direct fit of its spectral shape to the observed spectra. The results are reported in chapter 5 and compared to the spectral parameters obtained fitting other (canonical) spectral functions. The violation of the synchrotron limit in these spectra is discussed.

Possible alternative scenarios for the GRB prompt emission, based on synchrotron theory (Lloyd & Petrosian [99], Medvedev [107]) or on Comptonization (Brainerd [12], Liang [97], Ghisellini & Celotti [55]), have been proposed to justify the violation of this limit and the totality of the observed spectral properties, and they are summarized in chapter 3.

Although these models allow for the existence of spectra harder than $E^{1/3}$, they predict other limiting slopes which can be compared with the observations. In this sense we searched for the hardest spectra observed by BATSE which can constrain these alternative models. 5 bursts with low energy spectral slopes harder than E^0 are analyzed in chapter 6. Their hardness is verified with different tests in order to derive robust constraints which are compared and discussed within the above emission models.

The particularly hard low energy spectrum of some of these bursts ($F(E) \propto E^2$) results to be even consistent with a thermal black body spectrum. This was tested systematically on all the spectra of the bursts reported in chapter 6 and found to reasonably fit the initial phases of these GRBs. The interpretation of these results, within the context of the photospheric or Compton drag model, is detailed in chapter 6.

The other aspect which emerged from the time resolved analysis of this sample of bright bursts is the presence of different spectral evolution morphologies. The variability of the low and high energy spectrum of GRBs on small timescales (Ford et al. [42]) and the complexity of the spectral evolution have been reported by different authors (Crider et al. [23], Preece et al. [129]) through the study of the temporal evolution of the peak of the spectrum.

A different approach which describes the spectral evolution in terms of the complete set of parameters, obtained fitting the observed spectra, is proposed in chapter 7. The correlations of the spectral parameters with the flux are explored and the spectral evolution morphologies, revealed by this analysis, are discussed.

The Conclusions summarize the main implications of these results on the physics of GRBs, and outlines the opportunities of studying their spectral properties with unprecedented spectral coverage and time resolution, offered by the forthcoming missions (AGILE, GLAST, SWIFT).

Most of the content of this thesis (chapter 5 and 6) is part of published and submitted papers:

Ghirlanda G., Celotti A., Ghisellini G.
Time resolved spectral analysis of bright Gamma Ray Bursts
2002, Astronomy & Astrophysics, Vol. 393, 409.

Ghirlanda G., Celotti A., Ghisellini G.
Extremely hard GRB spectra prune down the forest of emission models
2002 to appear in A&A 406, 879.

and proceedings:

Ghirlanda G., Celotti A. and Ghisellini G.
Spectral analysis of Bright GRBs
2001 astro-ph/0112514
Proceedings of "Gamma-Ray Burst and Afterglow Astronomy 2001"
Woods Hole (MA) 5-9 November 2001

Tavani M, Band D., Ghirlanda G.
Time resolved GRB spectroscopy
"5th Huntsville Symposium"
Huntsville, Alabama, USA, 18-22 October, 1999.
Editors: R. Marc Kippen, Robert S. Mallozzi, Gerald J. Fishman.
AIP Conference Series, Vol. 526, 185

Chapter 1

GRBs: observations and theories

1.1 Introduction

This chapter describes the main characteristics of GRBs and of the theoretical models proposed for their interpretation. Exhaustive reviews on these subjects can be found in Piran ([126]), Meszaros ([114]) and Djorgovski [31].

In sec.1.2 are summarized the most important findings about gamma ray bursts obtained in more than 30 years of study: from the distance scale problem (sec.1.2.1), through the afterglow discovery (sec.1.2.3), to the most recent host galaxies analysis and their implications for cosmology (sec.1.2.4). Sec.1.3 outlines the standard model of GRBs and the internal/external shock scenario (sec.1.3.1). The possible progenitors, and their relation to the burst properties, are sketched in sec.1.4.

The spectral properties of GRBs, being the specific subject of this thesis, are presented in more details in chapt.2, whereas the emission models proposed for the burst γ–ray prompt phase, are detailed in chapt.3.

1.2 Observational evidences

1.2.1 The distance scale

Soon after their discovery, GRBs were interpreted as the transient emission of Galactic neutron stars. Unfortunately, this picture could not justify the isotropic sky distribution of a large sample of bursts observed by BATSE which opened the debate about the bursts origin. In fig.1.1 (*left panel*) is reported the angular distribution for 1637 GRBs in the 4B BATSE catalog[1], complete until 1996 (Paciesas et al. [118]): this distribution has a dipole moment $< cos\theta >= -0.025 \pm 0.014$ and a quadrupole moment $< sin^2 b - 1/3 >= -0.001 \pm 0.007$ which deviates 1.1σ and 0.4σ from the corresponding moments

[1] *http//cossc.gsfc.nasa.gov/batse/4Bcatalog/index.html*

of an isotropic angular distribution, opportunely corrected for non uniform sky coverage (Paciesas et al. [118]).

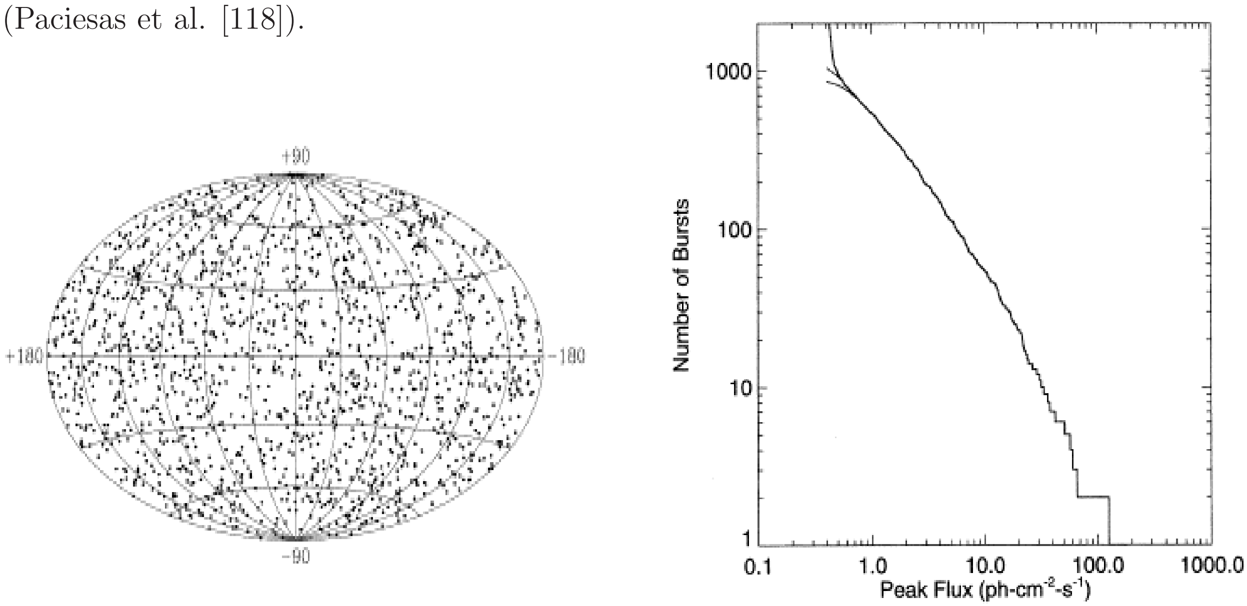

Figure 1.1: *Left*: distribution of the bursts of the 4B catalog with revised galactic coordinates. *Right*: peak flux distribution for bursts exceeding the 256 ms threshold. From Paciesas et al. [118].

A recent search for the untriggered bursts within the BATSE database (Kommers et al. [85]) has revealed a sample of 873 GRBs under the detection thresholds: these events, extending the sample of triggers, confirm the isotropic angular distribution of GRBs (with dipole and quadrupole moment -0.0029 ± 0.0195 and -0.0015 ± 0.0101, respectively).

The isotropic distribution of the bursts detected by BATSE might be consistent only with a population of sources which are distributed in an extended galactic halo or at cosmological distances.

The necessity of fixing the typical distance of GRBs was closely related to their energy reservoir which, in fact, is very different if they originate within the galaxy or at cosmological distances. An important BATSE result which, combined with the above distribution favored the cosmological distance scale (Paczynski [120]), is the peak flux distribution: in fig.1.1 (*right panel*) is reported the cumulative distribution of the flux (photon cm^{-2} sec^{-1}), at the peak of the light curve, accumulated on 256 ms timescale for the bursts of the 4B catalog. It shows a departure from the -3/2 slope predicted for an homogeneous distribution of sources in Euclidean space. The homogeneity test $\langle V/V_{max}\rangle \sim 0.32$ has a substantial deviation from the value (i.e. 0.5) predicted for the same homogeneous population of sources distributed in Euclidean space, and this, combined with the deviation of the LogN–LogS at low fluxes, favours the cosmological nature of GRBs. The final and conclusive evidence that GRBs originate at cosmological distances was the first redshift measurement of GRB 970508 (Frail et al. [43]) at z=0.835. This was followed by an increasing number of bursts with associated redshift and the actual z distribution (excluding the case of GRB980425 associated with the the relative close by supernova 1998bw at $z \sim 0.008$, Galama et al. [48]) extends from 0.4 to 4.5.

1.2.2 Temporal properties

The light curves of GRBs reveal a wide range of temporal characteristics: they last from few seconds to kiloseconds and present extremely different intensities and morphologies.

The duration distribution, defined with the T_{90} parameter[2] and reported in fig.1.2, shows a bimodality with a separation at about 2 sec (Kouveliotou et al. [86]). This is considered a signature of the possible existence of two different populations of bursts: long GRBs, lasting more than 2 sec (with a typical duration around 10 sec), and short bursts (about a third of the total) with $T_{90\%} \leq 2$ sec (Mitrofanov et al. [115]). This bimodality was confirmed also by the associated spectral shape, since short bursts, on average, appear harder than long ones. Moreover, these duration separation has been suggested to reflect a possible different origin for long and short bursts, i.e. the single star core collapse or the binary merger (Fryer et al. [45]), although this theoretical prediction still need a confirm.

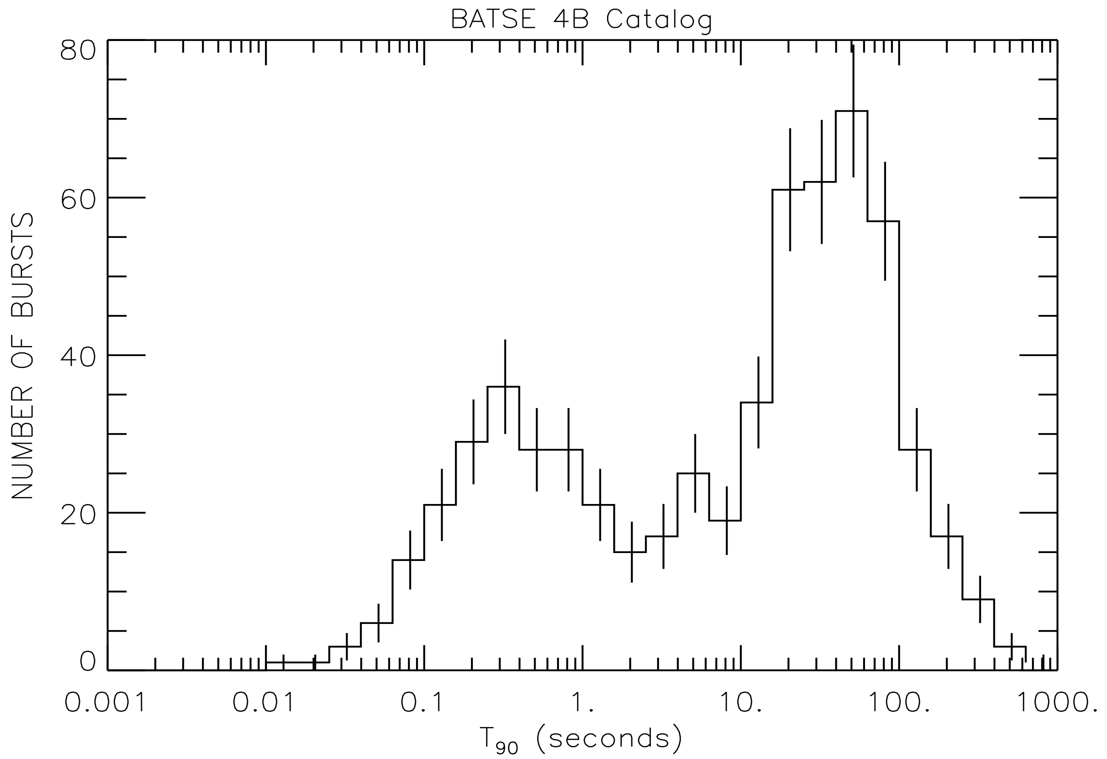

Figure 1.2: Duration distribution (T_{90}) for the bursts of the 4B catalog (Paciesas et al. [118]).

The GRB light curves have different morphologies and cannot be easily classified

[2] $T_{90\%}$ is the time interval containing the 90% of the burst fluence

according to a simple scheme (Fishman & Meegan [38]) although there are evidences that the burst pulses might be represented by a stretched exponential function (Norris et al. [117]) $N(t) \propto exp(-[(t-t_{max})/\sigma_{r,d}]^{\nu})$, where t_{max} represents the time of the pulse peak, $\sigma_{r,d}$ is the rise or decay constant and ν is a measure of the peakedness of the function. This expression has been fitted to samples of pulses and Norris et al. ([117]) have found that the decay phase is mostly represented by a pure exponential ($\nu = 1$) or a gaussian tail ($\nu = 2$). These results have been confirmed by Li & Fenimore ([93]) through direct fitting of this function to single spikes in highly variable light curves. Their analysis also showed that the rise phase is typically faster than the decay, confirming the FRED (Fast Rise Exponential Decay) temporal morphology.

The light curve of GRBs is also erratic and the flux can vary significantly on very small timescales. This burst variability is typically of 1 – 4 ms with a minimum of 0.2 ms (Schaefer & Walker [148]) and represent a constraint for the burst models (Walker et al. [159]). In multipeaked bursts the variability timescale is invariant from the beginning to the end of the burst (Ramirez-Ruiz & Fenimore [132]). The short and invariant timescale of the burst emission would favor the internal shock scenario because it associates the observed variability to the distribution of the Lorentz factors of the colliding shells. In the external shock model, instead, the decrease of Γ, due to the interaction with the ISM, would produce a stretching of the variability timescale in late pulses.

Recently, Fenimore & Ramirez–Ruiz ([37]) have shown that the variability measure, for a sample of bursts, is significantly anti–correlated with their absolute luminosity: smooth bursts are intrinsically less luminous. This relation, if confirmed, could be used to determine the GRBs redshift, only from their temporal properties.

1.2.3 The Afterglow

The Afterglow of the burst is its emission in the X-ray, optical, IR and Radio band. GRB 970228 is the first γ–ray burst for which an optical counterpart was found (Costa et al. [17], Frontera et al. [46]) thanks to the fast and precise determination of its position in the WFC. The optical transient, a 21st magnitude source in a position consistent with the γ ray detection (van Paradijs et al. [124]), was embedded in an extended object (Groot et al. [64]), i.e. the host galaxy. Subsequent HST observations showed the typical power law decay in flux of the Optical Transient (OT) and determined its redshift z=0.695 (Djorgovski et al. [31]).

The light curve of the optical afterglow of GRB 970228, 2 weeks after the burst, shows a deviation from a pure power law (fig.1.3): this was speculated to be a possible signature of the presence of a SN type Ic whose flux, as possibly shown in fig.1.3 (Galama et al. [49]) becomes important when the afterglow is dim enough. Observations of GRB afterglows span a broad range of frequencies, roughly form $\sim$ 1 GHz to 10^9 GHz, and timescales from hours (or even minutes) to a few years after the burst. Their broad band light curves, as shown for example in fig.1.4 , convey useful informations on the afterglow and also on the nature of the progenitor. As shown in the examples reported in fig.1.4

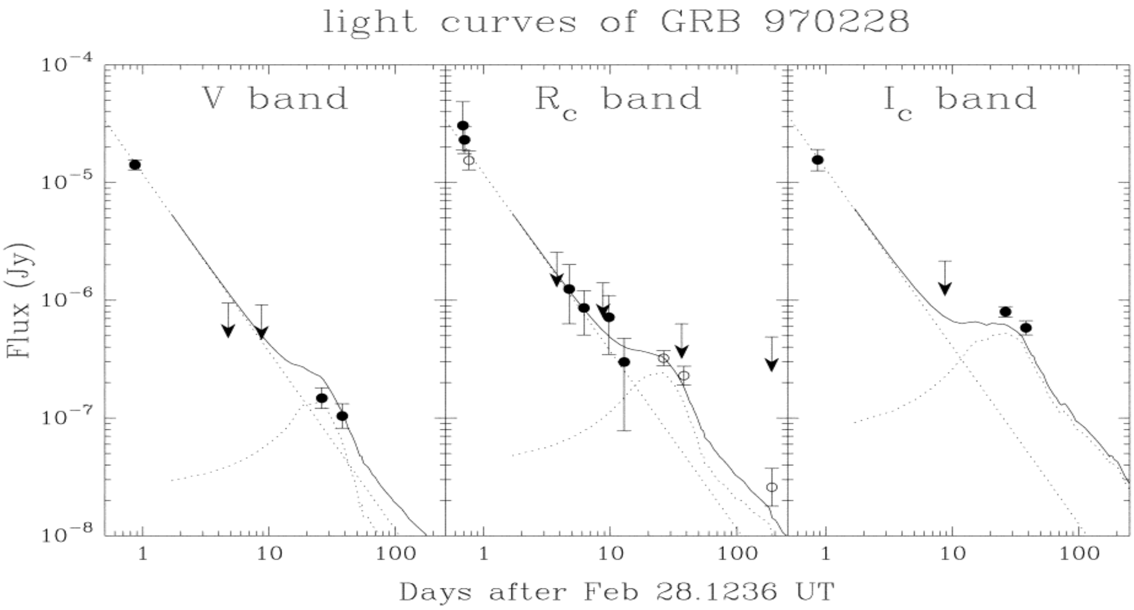

Figure 1.3: Light curves of GRB 970228. Dotted curves indicate power-law decays with index -1.51 and the redshifted SN 1998bw light curve. From Galama et al. [49]

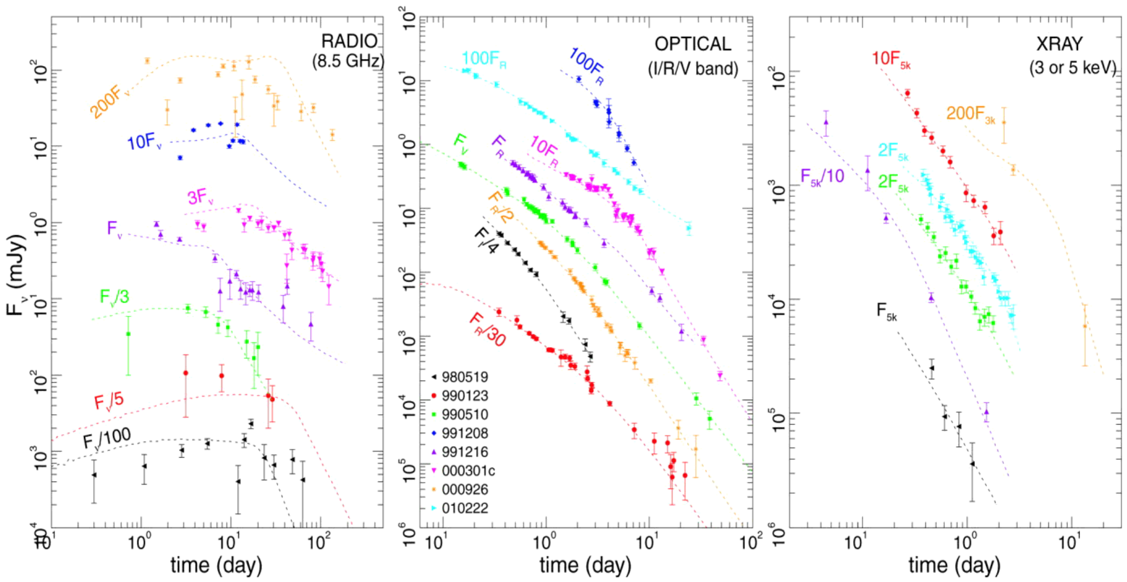

Figure 1.4: Radio, optical, and X-ray emission and model light curves for the GRB afterglows 980519, 990123, 990510, 991208, 991216, 000301c, 000926, and 010222. Optical data have been corrected for Galactic dust extinction. Fluxes have been multiplied by the indicated factors, for graphical purposes. From Panaitescu & Kumar [122]

(from Panaitescu & Kumar [122]), the afterglow light curve is often modeled by a single or a multiple power law which has its natural explanation in the context of the external shock model as due to the deceleration (Γ decrease) of the expanding shell by the ISM.

From these data, Panaitescu & Kumar ([122]), propose that the kinetic energies involved in the afterglow phase (i.e. still available after the GRB) are clustered around a mean value of 3×10^{50} erg.

Another consequence of a possible analysis of these data is that they could imply jet apertures of $\sim 2°$ For all the eight afterglows reported in fig.1.4, the total energy in the shock–accelerated electrons, according to the standard external shock model, is close to the equipartition value and the slope of the power-law electron energy distribution varies between 1.4 and 2.8. The implied densities of the medium are $\sim 0.1 - 50$ cm^{-3} with the exception of GRB 990123 which, according to the analysis of Panaitescu & Kumar ([122]), indicates a density of 10^{-2} cm^{-3}. Such low densities could find a possible explanation in the super bubble model (Scalo & Weeler [146]) although observational evidence is still required to support this theory.

Interestingly, the deviations and complications of the simple power law shape observed in several broad band afterglows, and partly determined by observational limitations, represent useful tools for the determination of some physical properties of the afterglow environment:

- interstellar scintillation, which affects the radio observation, has been used to resolve the afterglow size (Frail et al. [43]) in the case of GRB 970508;

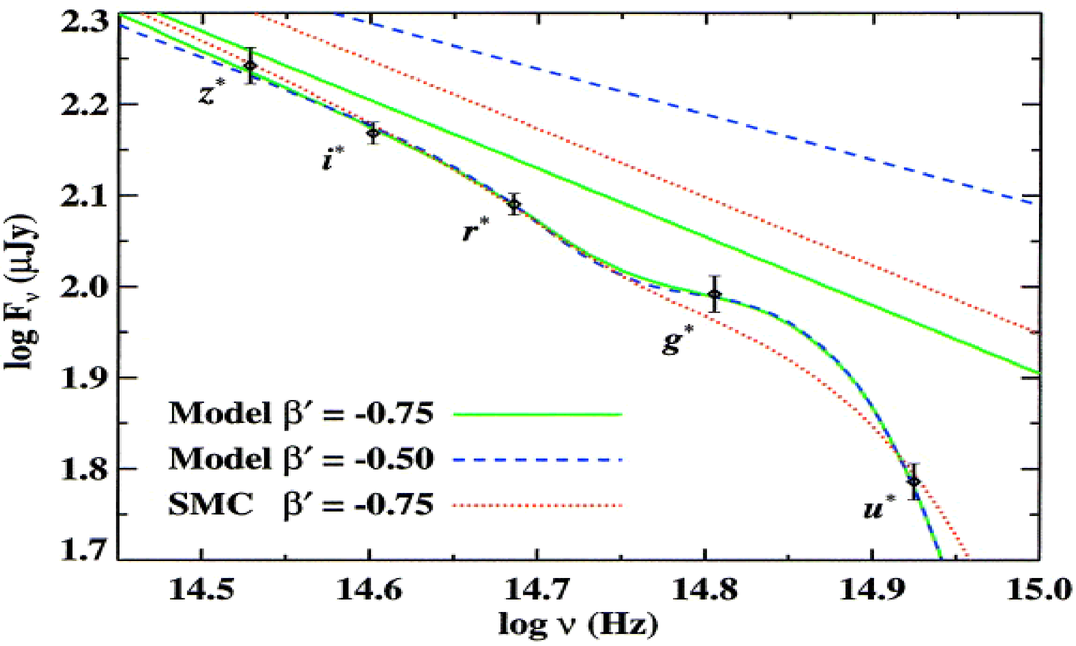

Figure 1.5: Multi-band observations of GRB 010222. The solid and dotted curves through the data points correspond to the extinction model fit for z = 1.477 and a source spectrum with slope of $\nu^{-0.75}$ (green solid curve) and $\nu^{-0.5}$ (blue dashed curve). From Lee et al. [92].

- extinction in the optical and NIR (corresponding to the UV rest frame), which alters the observed optical light curve, provides informations on the GRB environment: Lee et al. [92] report the multicolor observations of GRB 010222 (fig.1.5), corrected for reddening and for the afterglow temporal decay, and suggests that they can be reasonably fitted by a power law $F \propto \nu^{-0.90\pm0.03}$ with the exception of the UV (fig.1.5, u^* measure) which mostly suffers from the dust extinction of the star forming region in which the burst exploded.

- the inverse Compton scattering, which can dominate the electron cooling and produce an excess in the X–ray band, can provide an estimate of the density of the medium: Harrison et al. [68] report the broad band light curve of GRB 000926, and, though the model is quite complex, if compared to the low number of data points at high energies, they suggest that the X–ray data are consistent with the presence of an IC component (fig.1.6).

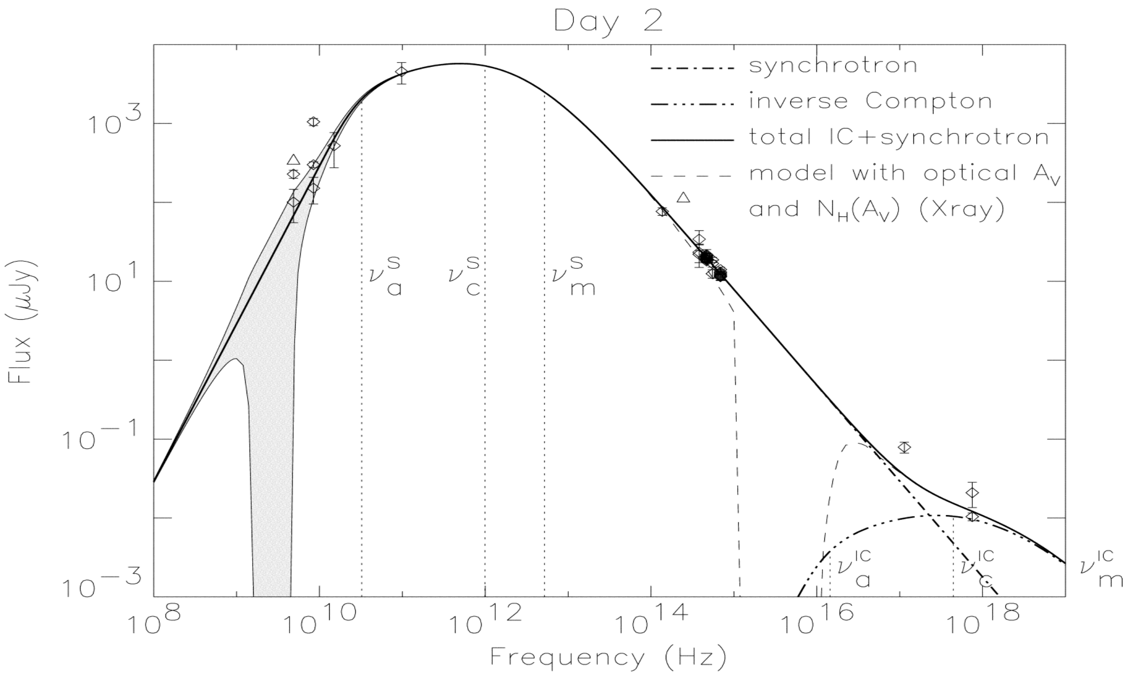

Figure 1.6: Broad-band spectrum of the afterglow of GRB 000926, two days after the jet break. The data, corrected for host extinction, are shown by diamonds, with their 1σ errors, the solid line is the best-fit model without host extinction, and the dashed line shows model plus extinction. The locations of the synchrotron spectral breaks, associated with self-absorption, cooling, and the maximum electron energy, respectively, are indicated. The IC component (*dot-dashed line*) in the right hand corner contributes the X–ray excess of the early afterglow. Form Harrison et al. [68]

Detecting the IC emission in the X-ray band directly implies a lower limit on the density (Sari & Esin [145]) which, in this case, results $n = 30$ cm^{-3}. This value is higher than the average ISM density in a typical galaxy and is consistent with a diffuse interstellar cloud, as those commonly found in star-forming regions. Combining the density with the host column density N_H derived from optical observations and assuming typical dust-to-gas ratios, Sari & Esin ([145]) derive a 2 pc size for the cloud. These results have been suggested as additional possible evidence of the association of GRBs with SF region.

- the presence of a host galaxy (sec.1.2.4) which may obscure the afterglow at late times, can provide better estimates of the star formation rate: late-time observations of GRB 980703 by Berger & Kulkarni [7], for example, revealed a steady radio component, with a flux density $F(1.43\text{GHz}) = 68.0 \pm 6.6$ Jy and spectral and temporal signatures typical of star forming regions. This led to the interpretation that this host galaxy is a Ultra Luminous Infra Red Galaxy, undergoing a starburst, likely concentrated within its inner 3 kpc.

These are just few examples indicating how the observations of GRBs in different bands and the analysis of their environments can provide important constraints on their physical parameters.

Another feature of the afterglow radiation is its polarization: synchrotron emission, in fact, should reach a level of 60% of polarization for ordered magnetic fields, which might be observed as 10%-20% if the emission occurs within a collimated outflow. This percentage of polarization is lowered in the case of GRBs due to the averaging of the polarimetric measure on unresolved sources (de–polarization effect). Hjoth et al. [70] report an upper limit for the R band polarization of 2.3% in the case of GRB 990123. Another measure comes from GRB 990510 (Covino et al. [19]) with a polarization of 1.7±0.2. Such low level of polarization has been suggested to be possibly produced by a magnetic field which is highly tangled, because generated by some instability (Gruzinov & Waxman [66]), or due to the aberration effects of the ring shape of the emitting region (Ghisellini & Lazzati [53]).

The discovery and analysis of emission lines in the GRB X–ray afterglow (Piro et al. [127]) provide constrains on the line–emitting material (Ghisellini et al [59]). These lines are usually identified as iron K_α emission features with an estimated energy $\sim 10^{49}$ erg, which implies a γ–ray energy, responsible for the ionization of the medium and of the consequent line emission, of 10^{51} erg. This value represents a lower limit for the burst energy derived independently from the beaming or collimation argument (Ghisellini et al [59]).

1.2.4 Hosts and Cosmology

The galaxies which host GRBs provide insights on the burst source:

- they allow to study the environment in which the GRB occurs and in which its progenitor evolved;
- they can be used to measure (or confirm) the redshift of the GRB, especially when too late afterglow detections do not allow a spectroscopic absorption line identification or when the OT is not detected;
- the displacement of the OT with respect to the center of the host provides useful information about the GRB progenitor and its association with star forming regions.

The observations in the visible (UV rest frame) are particularly difficult, due to the large intrinsic and galactic extinction. The absolute magnitudes, determined from the R band, assuming a power law spectrum with index -1 and no extinction correction (Djorgovski et al. [30]), show that the hosts of GRBs are sub luminous relative to present day luminous galaxies with possible implications for GRB–star formation association.

The sample of host galaxies , complete to GRB 010222, indicates a median apparent magnitude R$\sim$24.8, with a possible upper limit R$\sim$29. Down to R$\sim$25 the magnitude distribution is consistent with deep field galaxy counts (Smail et al. [150]).

The analysis of the star formation rate (through the [O II] 3727 doublets and UV continuum at 2800 Å or the Lyα 1216 Å line - which are all susceptible to the extinction within the host galaxy) indicates that it ranges from a few tenths to a few $M_\odot\ yr^{-1}$ which is typical for the normal field galaxies, at comparable redshifts.

The host galaxy morphologies seem to favor the late and irregular type, as shown by the analysis of 20 hosts by Bloom et al [10] in which it is found that the most close–to–center GRBs have blue compact and irregular hosts, which are indicative of intense star formation. Some examples of hosts are reported in fig.1.7 with the positional circle of the associated GRBs.

The GRB offset, with respect to its host center, shows that bursts (at least the long GRBs for which the hosts have been observed) are within some Kpc from the galaxy center: this could favor the massive star progenitor with respect to the binary system because, in the latter case, the system would be characterized by a large proper velocity and, consequently, the burst should occur far from the formation region.

Finally, GRBs represent a very powerful tool for cosmological studies. In fact, if long bursts are produced by the collapse of massive stars, one expects to find them out to z$\sim$ 15 - 20 (Lamb [88]). Therefore GRBs could give information about the star formation history of the universe and on the first generation of stars. Moreover, the absorption–line systems and the Lyα forest visible in the spectra of GRB afterglows can be used to trace the evolution of the metallicity in the universe and to probe its large scale structure.

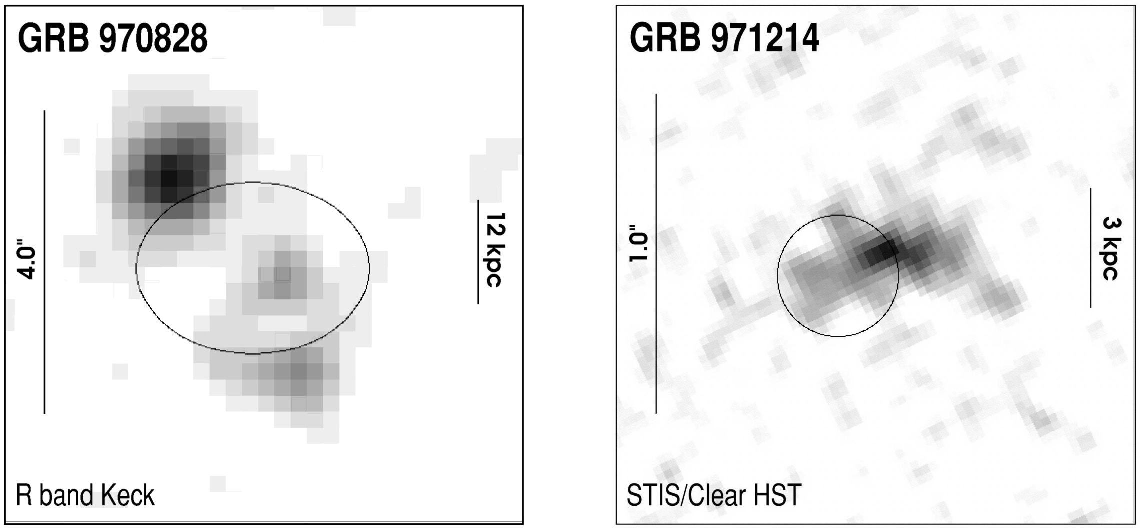

Figure 1.7: Some examples of host galaxies and related GRB error box, from Bloom et al. [10].

Nonetheless, measurements of the Lyα break in the afterglow spectra can constrain the reionization epoch.

1.3 The Standard Model

The observed GRB fluxes, at cosmological distances, imply a release of energy $\leq 10^{54}$ erg (assuming isotropic emission). The observed variability timescale $\delta t \sim 1$ ms indicates typical size of the emitting region $r_{min} \sim c\delta t \sim 10^7$ cm. The confinement of such a huge amount of energy, mostly in photons, in a small volume is called a *fireball.* within this volume a lot of pairs would be produced due to the high optical depth:

$$\tau_{\gamma\gamma} = \frac{f_p \sigma_T F D^2}{r_{min}^2 m_e c^2} = 10^{13} f_p F_{(-7)} D^2_{3000Mpc} \delta t^{-2}_{1ms} \tag{1.1}$$

where f_p represents the fraction of photon couples which satisfy the condition for $e^{\pm}$ production (i.e. $\sqrt{E_1 E_2} > m_e c^2$) and F and D are the fluence (in erg/cm^2) and the distance expressed with fiducial values. This opacity is extremely high for a burst with a 10^{-7} erg/cm^2 fluence at 10^3 Mpc with a variability timescale of 1 ms such that no high energy photon would escape from this thick fireball. This apparent paradox, i.e. the impossibility of releasing γ–ray photons which are indeed observed in the GRB, is known as the *compactness problem* (Goodman et al. [61], Paczynski et al. [119]) and was solved considering that the fireball expands relativistically with Lorentz factor $\Gamma = 1/\sqrt{1 - v^2/c^2}$. In this case the photons, observed with energy $h\nu$, have a lower energy in the source rest frame, i.e. $h\nu/\Gamma$, and, consequently, the fraction of photons which can produce pairs is reduced at least by a factor Γ^2 (if their spectral energy distribution is a powerlaw with slope -1). Similarly, the radius of the emission is $r_{min} \leq \Gamma^2\ c\delta t\ \Gamma^2$. Allowing for these relativistic effects, the resulting optical depth is

$$\tau_{\gamma\gamma} = \frac{f_p \sigma_T F D^2}{\Gamma^{2\alpha+4} r_{min}^2 m_e c^2} = 10^{13} f_p F_{(-7)} D^2_{3000Mpc} \delta t^{-2}_{1ms} \tag{1.2}$$

and the Lorentz factor required to make the fireball optically thin to pair production ($\tau_{\gamma\gamma} \sim 1$) results $\Gamma \geq 100$.

The expansion with a large Lorentz factor is limited by the baryon loading of the fireball (Shemi & Piran [149]) : if the baryon content is large, most of the fireball internal energy will be transferred to the baryons which, will gain only newtonian velocities. The baryon loading is typically parametrized as $\eta = E_0/M_0c^2$ where E_0 and M_0 are the fireball initial energy and mass.

If the fireball is intially dominated by its internal energy (a possible alternative is the a fireball driven by magnetic energy, e.g. Spruit [151]), its evolution is radiation dominated and, assuming adiabatic expansion, the bulk Lorentz factor Γ increases with r while the comoving temperature T scales as r^{-1}. Obviously, Γ cannot exceed $\Gamma_0 = E_0/M_0c^2 = \eta$ and this acceleration phase is then followed by a coasting phase with constant bulk Lorenz factor.

The intial expansion of the thick fireball determines the thermalization of its components (radiation and matter). When the fireball has expanded enough and becomes transparent (i.e. $\tau \leq 1$) it should release the bulk of its radiation in form of thermal photons with a black body spectrum. Nonetheless, the observational evidence that GRB spectra are non thermal (see chapt.2) required the formulation of an efficient mechanism for the extraction of the internal energy and for its subsequent transformation in non–thermal radiation. This is realized in the Internal/External shock scenario.

1.3.1 The fireball: internal/external shock model

In the coasting phase the possible difference of the Γ of different shells (or of different regions within the continuously ejected wind), can determine their collision which produces the *internal shocks* (Rees & Meszaros [133]). Very approximately, if shells are emitted with differences in their Lorentz factors $\Delta\Gamma \sim \Gamma$ then the typical radius of the internal shock formation is:

$$r_{IS} \sim c t_{var} \Gamma^2 \sim 3 \times 10^{14} t_{var} \Gamma_2^2\ \ cm \tag{1.3}$$

where t_{var} is the variability timescale (of the order of milliseconds).

The internal shock, then, converts the kinetic energy of the fireball into random energy of the particles which are accelerated by successive shock crossings. These particles are responsible for the emission of synchrotron radiation due to the presence (or formation) of an intense magnetic field. This process, together with its alternatives, for the production of the γ–ray emission of bursts are described in some details in chapt.3.

The internal shock is followed by the interaction of the ejecta with the interstellar medium which decelerates the shells and produces the *external shock* (Meszaros & Rees [110]) This, in a similar way, transfers its energy to the electrons which subsequently radiate through synchrotron, producing the afterglow emission (Sari et al. [142]). The condition for the formation of the external shock is that the swept up material is M_0/Γ and the radius at which it happens is:

$$r_{ES} \sim 10^{17} E_{53}^{1/3} n_0^{-1/3} \Gamma_2^{-2/3} \quad cm \tag{1.4}$$

where n_0 is the external medium density.

The external shock luminosity is $\propto t^{-1+g}$ with the Lorentz factor $\Gamma \propto t^{-g/(1+2g)}$ (g=3 or 3/2 for the radiative or the adiabatic case, respectively). As the synchrotron characteristic frequency is $\nu_m \propto \Gamma B' \gamma_e^2$, both B' and γ_e^2 are proportional to Γ and the peak of the emission moves to longer wavelengths. Meszaros & Rees [112] calculate that the afterglow flux and frequency dependence, as long as the expansion is relativistic, are:

$$F_\nu \propto t^{-3\beta/2} \quad , \quad \nu_m \propto t^{-3/2} \tag{1.5}$$

under the adiabatic assumption.

1.4 Progenitor

The greatest unknown in GRB science is what is the progenitor of the burst. There is no direct observable which can unveal the nature of the central engine but only an incomplete set of observational evidences about the GRB prompt and afterglow phase which should be used to infer the identity of the progenitor.

Any progenitor model should deliver few 10^{51} erg in relativistic collimated (≤ 0.1 radiant) ejecta in form of a continuous wind or of discrete shells with highly variable Lorentz factor. The variety of light curves (single/multi-peaked) and durations (short/long GRBs) could reflect a variable progenitor or a variety of progenitors and the study of the host galaxies and of the burst environments suggests a possible association between GRBs and star forming regions.

At present there are two main classes of proposed progenitors of GRBs: the *collapsar model* where a single massive star core–collapses to form a Black Hole (BH) surrounded by a torus, i.e. the (Woosley [162], Paczynski [121]), or the double compact object merger in which a binary Neutron Star (NS) or a NS-BH system undergoes a merger and forms a BH surrounded by an accreting torus (Goodman [61]). Both models produce, as a final result, a fast spinning BH surrounded by a very dense neutron rich torus and their energetic content is quite similar. The main phases associated with these models are: the progenitor evolution until the formation of the disk-BH system and the energy extraction to form the pair-radiation fireball which then produces the burst

The available sources of energy, a part from gravitational radiation, are in the form of neutrinos, accretion of the torus material onto the black hole, and rotation of both the torus and BH.

The mechanisms for the extraction of the energy are:

1. energy extraction from the torus (Woosley [162]):
   - one energy source is the binding energy of the torus which by viscous dissipation produces an intense neutrino flux and by annihilation an e^+e^- fireball. This mechanism can extract up to 10^{50-51} erg, which is consistent with recent estimates by e.g. Frail [44], Ghisellini [58];
   - an alternative method is the dissipation of magnetic fields generated by the differential rotation of the torus (e.g. Katz J. [78]). In this case the energy is
   $$E_d \leq 8 \times 10^{53} \epsilon_m q \frac{M_d}{M_\odot} \tag{1.6}$$
   where $\epsilon_m \leq 0.3$ is the efficiency and q the BH rotational parameter. The torus mass $M_d/M_\odot$ ranges from 0.01 to 1, for the double or single star scenario (Paczynski [121]);
2. energy extraction from the BH e.g. through the Blandford–Znajek (BZ) mechanism (Blandford & Znajek [9]). In this case the energy extracted is comparable to the previous value (Meszaros & Rees [111]):
   $$E_{BH} \leq 5 \times 10^{53} \epsilon_m \frac{M_{BH}}{M_\odot} \tag{1.7}$$
   where ϵ_m and M_{BH} are the efficiency and BH mass, respectively. The BZ mechanism can produce bursts with similar energy content whereas the extraction of the torus binding energy or of the BH rotational energy can power bursts with different energy content (Meszaros [114]).

Collapsar

A collapsar (Woosley [162]) is a massive ($M > 40M_\odot$) rotating star whose core collapses to form a black hole, while the infalling outer layers, due to the high angular momentum, form a centrifugally supported disk. The faster accretion along the rotational axis of the BH creates a depletion funnel, while the disk accretes at a rate of 0.1 $M_\odot sec^{-1}$. For the first 10 - 20 sec the accretion of matter onto the BH produces (e.g. assuming the first energy extraction mechanism) a huge neutrino flow ($\sim 5 \times 10^{53}$ erg) which annihilate to form pairs. These pairs are conveyed within the funnel producing the outflowing jet of high Lorentz factor ($\Gamma \geq 200$) that escapes from the central engine along the polar axis and powers the GRB prompt and afterglow phase.

Two essential ingredients for the collapsar model are a sufficiently massive core to form a BH and a sufficient rotation rate at the time of collapse to allow the formation of the disk. Simulations of the collapsar model (MacFadyen & Woosley [101]) suggest that large angular momentum and a core mass $M_{He} \geq 10 M_{\odot}$ are required. Moreover, the propagation of the relativistic jet through the hydrogen envelope of typical massive stars is of the order of 100 sec. This requires that the star has already lost (through wind-mass loss or due to the gravitational stripping of a companion) most of its H envelope, which, otherwise, could prevent the jet to penetrate it on timescales comparable to the GRB duration (Haeger et al. [67]).

The collapsar scenario has different possible realizations which are characterized by the mass of the collapsing He core:

- Type I: $10 \leq M_{He} \leq 15\ M_{\odot}$. The black hole forms directly from the core–collapse.
- Type II: $15 \leq M_{He} \leq 40\ M_{\odot}$. The black hole formation is delayed by a time which is necessary to the initially ejected envelope to fall back.
- Type III: $M_{He} \geq 137\ M_{\odot}$. These values correspond to the Pop. III stars (primordial generation, Haeger & Woosley [67]), which (also without rotation) form a 100 $M_{\odot}$ BH. Their accretion rate is about 10 $M_{\odot}$ sec^{-1}, and the corresponding burst timescale would be 20 sec, in the comoving frame. The spectrum and duration of the resulting burst should be diluted for the redshift of these primordial stars so that, if at least some GRBs have these progenitors, they should be more likely detected as long X–ray bursts.

One key feature of the collapsar model is the formation of an accretion torus around the BH which is the primary energy source for the GRB. This can be prevented by the magnetic field and the mass loss during the core collapse which have been considered in recent simulations. The first, due to the differential rotation of the stratified star (Spruit [151]), can be more effective in the transport of the angular momentum than the hydrodynamic mechanisms and then produce (Haeger & Woosley [67]) a disk which is hardly supported by the centrifugal forces. The second effect undermines the disk formation because the mass loss rate carries away also angular momentum: a possibility to avoid this problem is considering low metallicity stars which are supposed to have lower mass loss rates.

Supranova

This model is a variant of the collapsar and was first proposed by Vietri & Stella [156]: it considers the implosion of a massive neutron star that has lost sufficient angular momentum (by gravitational radiation or magnetic torques) to collapse and form a BH. About 0.1 $M_{\odot}$ is left behind for the formation of the disk and the GRB powering (Vietri & Stella [156]). One immediate consequence of this model is the production of an environment surrounding the star rich in heavy elements which can be responsible of the

X-ray emission by illumination from the central object (Piro et al. [127]). Moreover, this model solves the problem of the heavy baryon loading (which could prevent the relativistic motion of the ejecta) because the SN explosion, which led to the formation of the NS, has swept most of the surrounding matter far from the center. This in turn requires that the NS to BH collapse occurred days/years before the GRB. But in this case the range of masses which can produce a SNe and such a delayed explosion is largely reduced (McLaughlin et al.[104]). Another problem could be the fact that the time necessary for the jet to drill the distant ejected envelope, might be longer than the GRB duration.

Double compact merger

The standard evolution of a binary system composed by two massive stars can lead to the formation of a compact object system which eventually merge producing the GRB. The merging system can be composed either by two NS or by a NS and a BH. A part from the details of the evolution and of the merger (e.g. Fryer & Woosley [45]), the double NS form a single object which is not supported against collapse by nuclear or degeneracy pressure and a BH is formed with a surrounding 0.03-0.3 $M_{\odot}$ disk whereas in the NS-BH the neutron star is disrupted by the BH to form an accretion disk of 0.1-1 $M_{\odot}$. The NS–BH evolution ($t \sim 10^9$ yr) leads to a final escape velocity of the compact system (due to the successive kicks determined by the explosions of the primary components during their evolution) of 100-1000 km sec^{-1} which would likely place the GRB outside the star forming region (Fryer & Woosley [45]).

Chapter 2

Spectral properties of GRBs

2.1 Introduction

The energy distribution of the photons emitted by Gamma Ray Bursts (i.e. their spectrum) is an observable directly associated with the burst prompt emission and represents the best tool for investigating the physics of the burst and its progenitor nature. The amount of energy released in the burst, the fraction which is converted into radiation in the Internal/External shock scenario, the dynamical and radiative timescales, mechanism producing the observed flux (chapt.3) and the interaction of the burst with its environment can be studied through the analysis of the temporal and spectral properties of GRB light curves and spectra.

Since their discovery, different instruments have been collecting an increasing amount of bursts with better temporal and spectral resolution (see chapt.4 - for an historical overview) and, consequently, the knowledge about GRBs properties has increased. Moreover, the refinement of the spectral analysis methodology has led to a more accurate definition of the spectral evolution of the burst. For this reason a description of the spectral properties of GRBs can be roughly subdivided into the pre–BATSE era (sec.2.2), when the spectral analysis of the first gamma ray bursts detectors posed the basis of the spectral characterization of bursts, and the BATSE era (sec.2.4), characterized by the study of large, statistically significant, samples of burst spectra, with improved resolution.

The aim of this chapter is to give a global review of the spectral properties of GRBs as a brief but specific introduction to the subject of this thesis. The typical shape of the spectrum and its temporal evolution are described in sec.2.4.1 and 2.4.2, respectively. A possible basic model, recently proposed, for the interpretation of these results is outlined in sec.2.5.

2.2 Definitions

The spectral properties of any GRB are strictly related to its typical timescales: the GRB has a global duration which can be quantified by the time interval containing the 90% of its fluence in [erg/cm^2] (defined as the time integral of the energy flux), and a short timescale, of few milliseconds, corresponding to the variability of its light curve. Other significant timescales can be identified e.g.: the duration of the pulses for multi–peaked bursts, the time in which the flux rises, reaching a maximum, and then decreases (rise/decay timescale).

For every timescale a corresponding category of spectra (e.g duration–integrated, pulse–integrated, etc.) can be obtained integrating the spectral signal, separated in different energy channels, over the selected time interval.

The spectrum

If $C(E,t)$ is the count spectrum accumulated by the instrument during the burst event per unit time and per unit energy, i.e. in [counts/cm^2 sec keV], its time integral defined the type of spectrum:

- *time integrated spectrum*, or time average spectrum, which is integrated for the duration (e.g. $T_{90\%}$) of the burst:

$$\overline{C(E)} = \int_{T_{90\%}} dt\ C(E,t) \tag{2.1}$$

  This spectrum, being integrated for some seconds (at least for the population of long bursts with $T_{90\%} \geq 2$ sec) has typically a good S/N and can be used to characterize the average spectral properties of GRBs and compare them among different bursts.

- *time resolved spectrum* which, despite its name, is integrated in time over a typical sub-second timescale (usually longer than the variability timescale t_v):

$$C(E) = \int_{t_v} dt\ C(E,t) \tag{2.2}$$

  The sequence of many time resolved spectra, covering the duration of the burst, describes the GRB spectral evolution. Integration over small timescales is limited by the S/N ratio of the time resolved spectrum. For this reason only particularly bright bursts, like those analyzed in chapt.5 (Ghirlanda et al.[51]), can be analyzed in terms of time resolved spectra on very short timescales (e.g. 128 ms, in the case of BATSE data). Integration over the rise/decay phase of the flux in the light curve defines, correspondingly, the *rise/decay phase spectrum*.

When dealing with the spectral properties of GRBs different notations can be found to indicate the spectrum and its representations: we denote the count spectrum in [count/cm^2 sec keV], the photon spectrum, which is $C(E)$ deconvolved by the detector response matrix (see. chapt.4), is indicated as $N(E)$ and has units of [photons/cm^2 sec keV]. The energy spectrum and the usual νF_ν spectra are indicated as $F(E)$ and $EF(E)$ and are expressed in [keV/cm^2 sec keV] and [keV (keV/cm^2 sec keV)].

A typical GRB spectrum is composed of two power laws connecting in correspondence of a spectral break: the low energy power law is conventionally represented as E^α and high energy power law as E^β, for the photon spectrum. The spectral indices α and β in the rest of these thesis indicate these two components and a negative value of these parameters indicate a photon spectrum which decreases with increasing energy.

Hardness

The characterization of the hardness of a burst can be associated with its spectral parameters (E_{peak},α,β), obtained fitting the observed spectrum with a model function or with its count rate:

- *peak energy*, E_{peak} which represents the energy corresponding to the peak of the νF_ν spectrum. This is a spectral parameter obtained from the fit of the observed spectra and indicates where most of the power is emitted. For GRBs it is often chosen to indicate the hardness of the spectrum. In terms of peak energy a spectrum is defined hard (soft) if its E_{peak} is high or low: $E_{peak} \sim 100$ keV describes a softer spectrum than $E_{peak} \sim 1$ MeV.

- *spectral indices*, α or β, which characterize the slope of the corresponding power laws. A burst spectrum is typically described at low energies by a power law with photon spectral index $\alpha \sim -1$. A larger value (e.g. $\alpha = -0.5$) characterizes a harder spectrum which in a log log representation is flatter than the previous case. The same definitions and nomenclature apply to the high energy spectral component described by β whose typical value is -2.5.

- *hardness ratio*, HR, defined as the ratio between the count rate (background-subtracted) in a high energy channel and the count rate in a low energy channel. It is directly obtained from the instrumental count and the resulting spectral hardness depends on the response of the instrument. A high (low) hardness ratio characterizes a hard (soft) spectrum.

These definitions of the spectral hardness of a burst have been largely adopted by different authors to describe the spectral evolution of GRBs, also for the simplicity to associate to a *single* parameter a measure of the hardness. Other possibilities can be considered, as suggested in chapt.7, which make use of the complete set of spectral parameters, e.g. E_{peak},α and β, to characterize the spectral hardness and its evolution over the complete energy band of the instrument.

2.3 Pre–CGRO era

Since the beginning, it was evident (e.g Cline & Desai [15]) that the spectrum of gamma ray bursts has a non-thermal shape well represented by a single power law or by a power law with an exponential cutoff (Klebesadel [84]). This experimental evidence opened the debate about the leading radiative process responsible for the GRB emission.

The spectral analysis of 6 bright bursts detected by the IMP-6 satellite (Cline et al. 1973) in the range 0.1-2 MeV showed that they could be reasonably well fitted by an exponential function $N(E) \propto E^0 exp(-E/E_c)$ with the e-folding energy $E_c \sim 150$ keV.

The IMP maximum time resolution was 2.5 sec so that particularly long bright bursts could be described by a sequence of some time resolved spectra. Although this was the first attempt to characterize the time resolved spectrum and its evolution, no evidence for a temporal variation of the spectral shape was found, probably due to the limited time and spectral resolution of these data. In fact, this analysis could not exclude the presence of an high energy spectral component, whose existence was later confirmed by Cline & Desai ([16]) through the study of 11 bursts detected by the IMP-7 satellite: some of these spectra, extending above 400 keV, had a typical power law shape $N(E) \propto E^{-2.5}$ at high energies.

The presence of an high energy spectral component was also confirmed by a larger sample of bursts (79) collected by the Solar Maximum Mission (SMM) in the energy range (0.3-9) MeV. The 66% of these bursts showed significant emission above 1 MeV and 25% even above 5 MeV (Matz et al [102]). These results supported the idea of representing GRB spectra with multiple components and, preferentially, with power laws at low and high energies, i.e. below and above a characteristic energy of some hundred keV.

The first study of the average and of the time resolved spectrum of GRBs revealed the different information conveyed by these two types of observables: Golenetskii et al. ([60]) analyzed the spectra of 150 bursts detected by the KONUS experiment, on board the VENERA 13 and 14 satellites, and found that the time integrated spectrum could be well represented by a power law $N(E) \propto E^{-1}$, at low energies, and an high energy exponential cutoff. The time resolved spectra (with a maximum resolution of 0.5 sec), fitted with the same spectral function, showed that the characteristic energy kT decreased with time and it was correlated with the intensity I. Golenetskii et al. ([60]) reported $I \propto kT^{\gamma}$ with γ=[-1.5,-1], and showed some evidences of candidates spectral lines, possibly evolving with time. The presence of line candidates in the γ–ray spectrum of GRBs was seemingly excluded by intense statistical analysis of the BATSE catalog by different authors (e.g. Band et al. [5], [6]).

The intensity–energy correlation $I-kT$ was also verified, with a better time resolution (0.25 sec), with the hardness ratio (HR) instead of the spectral parameter kT (Golenetskii et al. [60]). It should be stressed, anyway, that the HR (see sec.2.2 for a definition) is obtained from the count rate and is not deconvolved by the detector response matrix as in the case of the fitted spectrum. Moreover, HR should be considered a "rough" hardness estimate because it implicitly assumes that the spectrum is represented by a power law over a fixed energy band, without considering the curved and fast evolving GRB spectra.

Additional indications that burst spectrum can evolve in time according to some recurrent morphologies were given by the analysis of 10 bursts observed by the Hard X Ray Burst Spectrometer and Gamma Ray Spectrometer (Norris et al. [116]). They reported a hard–to–soft spectral evolution common to these burst: the hardness ratio and the peak energy decrease with time, since the beginning of the burst. Although the time resolution was only of 0.5-1 sec this evidence of an hard–to–soft spectral evolution apparently undermined the previous findings of an intensity–energy correlation. Still this morphology could have been determined by the low temporal resolution of these data (see chapt.7 for a discussion).

Nowdays, the increased time resolution of spectral data which allows to have a larger number of time resolved spectra per burst, confirmed that both these evolutionary morphologies characterize different GRBs.

The search for hardness–intensity correlation in GRBs was also performed by Kargatis et al. ([75]) with a sample of 16 bursts observed by SIGNE, a gamma ray detector with 0.5 sec resolution. They found both the hardness–intensity correlation of Golenetskii et al. ([60]) and the hard to soft evolution of Norris et al. ([116]), and, for the first time, gave a scheme of spectral evolution classification according to the following classes:

- *Hard–to–Soft* spectral evolution with the hardness indicator decreasing independently of the increase and decrease of the flux in the light curve;
- *Soft–to–Hard* spectral evolution which is the opposite of the one described before;
- *Tracking* morphology in which the hardness parameter reproduces the increase and decrease of the flux light curve.

As will be discussed in chapt.7, these morphologies can be present in different phases of the burst emission and in many cases the classification can be strongly biased by the time resolution of the spectral analysis.

2.4 The characterization of the GRB spectrum by BATSE

The Burst And Transient Source Experiment (BATSE) provided a fundamental contribution to the understanding of the GRB spectral properties because, accumulating a large sample of bursts with high spectral and temporal resolution (see chapt.4), allowed the comparison of the average spectral properties among different classes of bursts and the study of their spectral evolution.

The next sections describe the time integrated and time resolved spectrum of GRBs observed by BATSE. In particular, the average spectral characteristics of bursts are presented in sec.2.4.1, the time evolution of the spectrum and its low and high energy spectral shape are discussed in sec.2.4.2.

2.4.1 Time integrated burst spectrum

The burst spectrum, integrated over its duration as defined in sec.2.2, presents some basic features:

- it has a non thermal character which is evident from its low and high energy power law shape connected by a wide smooth curvature (Band et al. [4]);
- it can be fitted by an analytical spectral model, the BAND function (Band et al. [4]), which in most cases characterizes the peak of the νF_ν spectrum through its spectral parameters, giving a direct measure of the hardness of the burst;
- large samples of bursts present spectral parameter distributions (sec.2.4.2) indicating a prevailing spectral shape described by $N(E) \propto E^{-1}$, $N(E) \propto E^{-2}$ connecting at $E_{peak} \sim 300$ keV;
- there is no evident connection between the spectral properties and other burst properties (e.g. duration, position, intensity), as far as the time integrated spectrum can reveal;
- in few cases, data from the other CGRO instruments are available, the average spectrum extends above the typical 2MeV energy upper threshold of BATSE showing its non–thermal character also at high energies.

The analysis of a sample of 54 bright bursts by Band et al. ([4]) confirmed the non thermal character of the time integrated spectrum, which is well fitted by an empirical analytical form (defined in chap.5) composed by two power laws, at low and high energies, characterized by their spectral indices α and β, smoothly connected by an exponential cutoff with e–folding energy E_0. This spectral model (BAND, hereafter) has been extensively adopted to represent the burst spectra and, within the limits of its spectral parameters (α, β, E_{peak}), also accounts for the previously adopted spectral representation (e.g. single powerlaw with exponential cutoff, exponential function).

The search for correlations among the best fit parameters α, β (Band et al.[4]), only showed that they cluster in the ranges -1.5$\leq \alpha \leq$ 0 and -2.5$\leq \beta \leq$-2. Two examples of time integrated spectra and the relative GRB light curve are reported in fig.2.1 where the spectrum and the best fit BAND model are represented (*bottom panels*). Notice that they are both well fitted by the BAND model although the spectral parameters are different and in particular the peak energy is slightly different.

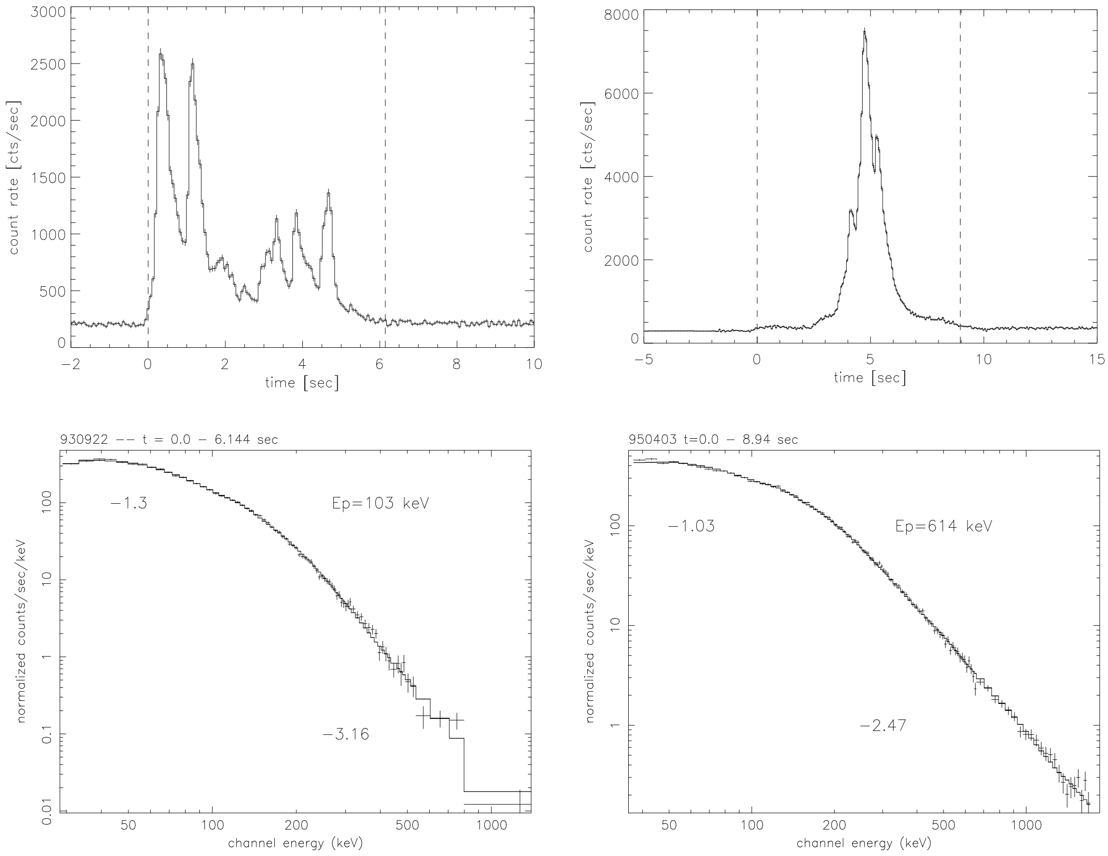

Figure 2.1: Examples of time integrated spectra. Left column: GRB 930922. Top panel: light curve with 64ms time resolution and integrated from 25 to 300 keV. Bottom panel: spectrum with best fit model (BAND) and relative parameters. E_p is the peak energy of the νF_ν spectrum, namely $E_{peak} = (\alpha + 2)E_0$. Right column: GRB 950403. The *dotted* vertical lines mark the time interval of accumulation of the spectrum.

In some cases extremely soft spectra at high energies (i.e. well represented by exponential cutoff components) were found although the low statistics of the high energy spectrum does not allow to definitely classify these spectra as a soft subclass.

The low energy spectral slope instead could be better studied because of the higher S/N ratio at low energies: Preece et al.([128]) analyzed a sample of 86 bright bursts considering also the hard X–ray data and then extending the low energy spectral threshold to 5 keV. Fitting the BAND model to the time integrated spectra they found a wide distribution of the α parameter, confirming the spectral diversity of the low energy spectrum among different bursts. They also report some extremely hard bursts, at low energies, with $\alpha > -2/3$ which call for an explanation within the proposed emission models. In fact, as it will be discussed in chapt.3, most of the radiative mechanisms, which have been thought to produce the spectrum of GRBs, make strong predictions on the slope of the low energy spectral shape. Until now, no exhaustive comparison of these

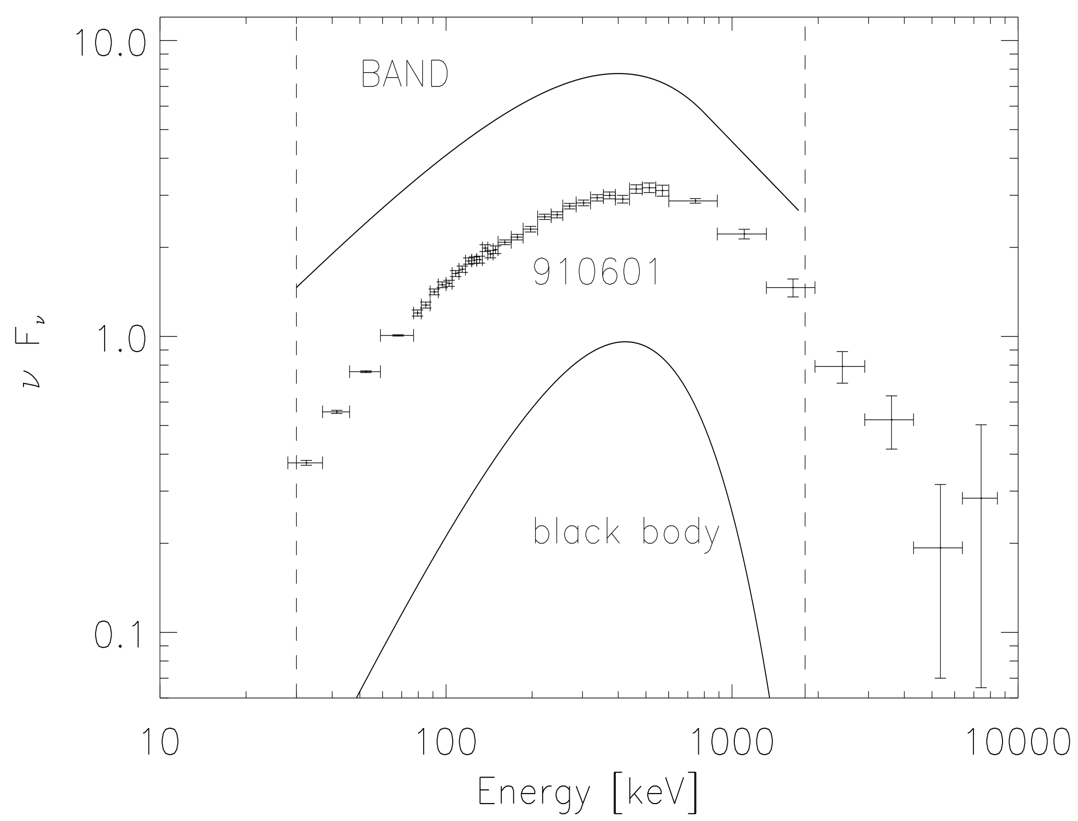

Figure 2.2: νF_ν spectrum of GRB910601. The BAND model with $\alpha = -1$, $\beta = -3$ and $E_{break} = 400$ keV is reported for comparison as representative of the non thermal spectral functions together with the black body spectrum with kT=150 keV. The *dashed* vertical lines represent the limits of the BATSE energy range. The data points are from Schaefer et al.([147]).

predictions with all the most significant experimental evidences has been attempted: we will consider this task in chapt.6 in the light of new results on some extremely hard low energy GRB spectra, discussing the proposed emission models.

Preece et al.([128]) report an anticorrelation between the low energy spectral hardness (indicated by the value of α) and the peak energy E_{peak}: bursts with hard low energy power law spectra ($\alpha > -1$) tend to have smaller E_{peak}. In most cases the spectrum at very low energies (below 30 keV) is consistent with the extrapolation of the fitted function in the gamma ray band although some exceptions, showing a low energy X ray excess, exist.

Although the BAND model is not based on any physical assumption, it gives a direct measure of the peak energy E_{peak} which is often used to characterize the hardness of the spectrum. Its distribution, as reported by Band et al. ([4]) for the time integrated spectrum, is log–normal and centered around $\sim 150 - 200$ keV and narrow. This last feature is extremely interesting if compared to the wide spread of the temporal properties of GRBs: some possible explanations of this peculiar narrow peak energy distribution are reviewed in sec.3.4.2.

The time integrated GRB spectrum has also been studied extending the BATSE energy range to some MeV with data from the other instruments on board the CGRO (Schaefer et al. [147]). They report 4 broad band (10keV - 100 MeV) spectra which are well represented by the BAND model. In fig.2.2 is reported, as an example, the case of GRB 910601 adapted form Schaefer et al ([147]). It is evident the power law shape of the spectrum, at low and high energies, and also its curvature, peaking at 300 keV. For comparison in fig.2.2 are also reported the BAND spectral model and the a black body spectrum (*solid lines*), with arbitrary parameters, as representative of the non–thermal and thermal spectral forms, respectively. It is evident that the broad band spectrum is better represented by a non-thermal model with a smooth curvature. Nonetheless, it might not be excluded that the spectrum, considered over a narrow band, can show, in some particular cases as those presented in chapt.6, a thermal character which indeed is hidden by the time integration of different spectral contributions over time. For this reason the best characterization of the spectrum is through its time resolved properties and their temporal evolution.

2.4.2 The spectral evolution

Considering the fast variability of bursts (e.g. Walker [159], Fenimore & Ramirez–Ruiz [37]), also the spectrum, as shown in this section, should be expected to vary on small timescales.

The study of the spectral evolution of a GRB is based on the temporal analysis of the hardness of the burst spectrum, once a definition of a spectral hardness indicator has been given (sec.2.2).

In principle the requirement of studying the variation of the spectrum on the smallest integration timescale (set by the instrument temporal resolution), is limited by the low statistics of γ photons, particularly at high energies. For this reason the experimental choices for the analysis of the spectral evolution have been subject to different refinements also in connection with the advances of the spectral accumulation techniques.

The mass of data collected by BATSE allowed to fix some major observational evidences about the spectral evolution:

- the time resolved spectrum has a non–thermal character;
- it can be well represented by the BAND function although there are some other spectral forms (e.g. COMP, SSM, BPLW model, discussed in chap.5) which can adequately fit the spectrum.
- the evolution of the spectrum described with the hardness ratio or with a best fit

spectral parameter, like the peak energy, can be classified according to the relation between the hardness evolution and the flux time history;

- there is a correlation between the burst hardness and its intensity (represented by different parameters);
- the low energy spectral slope of a considerable fraction of spectra violates the limit predicted by the standard optically thin synchrotron model ($\alpha = -2/3$);
- the high energy spectral component highlights the possible existence of super-soft or super-hard bursts which could likely represent sub populations of the burst phenomenon.

In the following sections these findings are presented in more details.

Spectral evolution morphologies

The first comprehensive study of the spectral evolution of a sample of bright bursts observed by BATSE (Ford et al. [42]) showed that in many cases the hardness indicator, e.g. the peak energy E_{peak}, rises and decays during the burst reproducing its light curve. The higher time and spectral resolution of BATSE data confirmed the existence of the hard-to-soft and tracking morphologies and added to the classification scheme some new evidences:

1. *tracking*: the peak energy and the burst intensity are correlated. The peak energy can reach its maximum value before or after the peak of the light curve, and this time delay is typically less than 1 second;
2. *hard–to–soft*: the peak energy decreases during pulses. In this class Ford et al. ([42]) included also those cases in which the peak energy maximum anticipates the light curve maximum by more than 1 sec.
3. *hard–to–soft inter pulse*: the tracking evolution dominates the peaks, while, during the quiet phases (inter-pulse), the evolution is hard–to–soft.
4. *envelope*: there is a general softening of the burst shown by the lower hardness of the late pulses with respect to the early ones.

This classification is based on the dominant morphologies but some exceptions exist, and different evolutionary types can characterize different phases of the burst.

In fig.2.3 are reported some examples from Ford et al. ([42]). In the case of GRB 910807 (top left panel) the peak energy follows the light curve (tracking) in the second peak but softens during the first peak: this is an example of coexistence of the two morphologies. Notice also that the second peak, although it is dimmer than the first, has the same hardness indicating the absence of the hard-to-soft envelope, which is

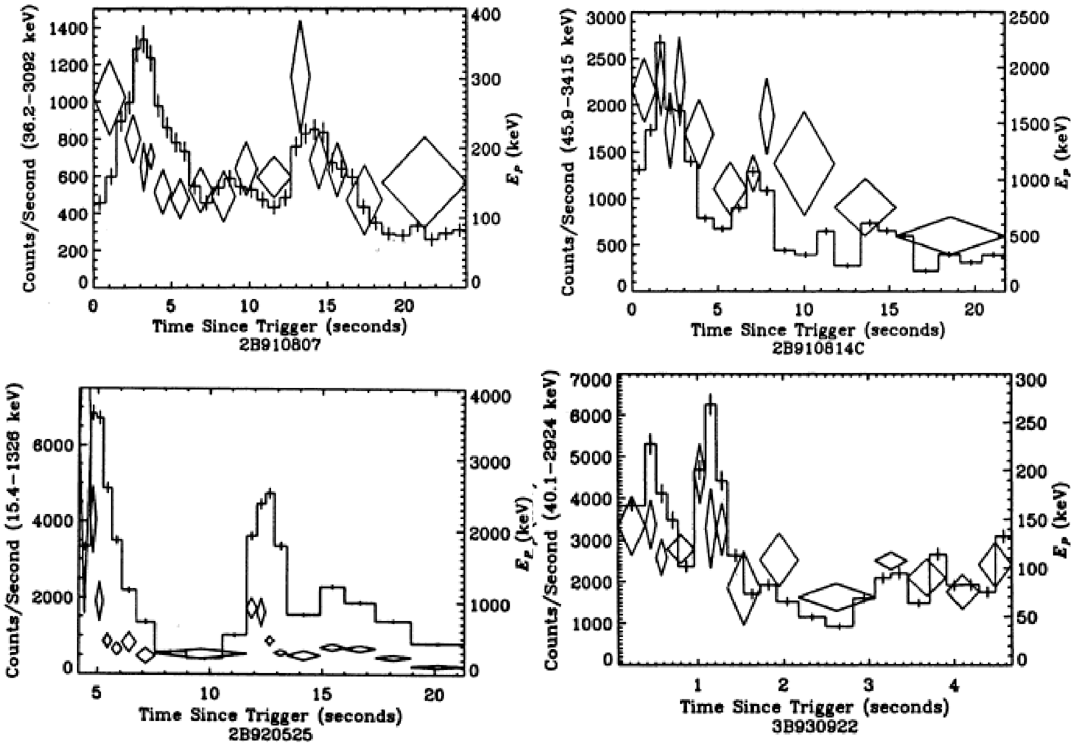

Figure 2.3: Examples of evolutionary morphologies from Ford et al. [42]. The light curve is reported (*histogram*) and the peak energy of the $\nu F\nu$ spectrum (*diamonds*) as a function of time.

instead present in GRB 920525 (bottom left panel). The simple hard–to–soft spectral evolution is shown by GRB 910814 (top right panel) in which E_{peak} decreases with time. GRB 930922 shows a hard to soft evolution during the second peak.

The evidence of the hard–to–soft envelope is shown also by the distribution of the peak energy of late spikes compared to that of early spikes: Ford et al. ([42]) found that for multi peaked bursts the late emission is systematically softer than in the first seconds of the burst. A possible quantification of this morphology, through the time resolved spectral analysis of the sample of bright bursts presented in this thesis, is actually under consideration and the first results will be detailed in chapt.7.

Spectral–temporal correlations

The quantitative description of the spectral evolution has been performed considering the possible correlations between the hardness parameter and the intensity of the burst (Kargatis et al. [76]) or the hardness and the fluence (Liang & Kargatis [94]). Ryde & Svensson ([137]) pointed out that these correlations can be used to derive an analytical function which can easily reproduce the observed light curves.

It should be stressed, anyway, that these analytical descriptions (Liang & Kargatis [94], Ryde & Svensson [137]) of the spectral evolution only apply to the decay phase of well defined long pulses, and then do not describe the spectral evolution before the burst peak, i.e. the initial phase of the emission. This is motivated by the fact that the rise phase is typically fast and characterized by a low S/N so that the number of time resolved spectra and their statistical quality is often less than in the decay phase.

The hardness (described by the peak energy E_{peak} of the νF_ν spectrum) was characterized by an exponential function of the fluence by Liang & Kargatis ([94]). They found, in a sample of 37 pulses, that the Hardness Fluence Correlation (HFC) could be described as:

$$E_{peak}(t) = E_{peak,0} e^{-\Phi(t)/\Phi_0} \tag{2.3}$$

where Φ represents the fluence and the constants, $E_{peak,0}$ and Φ_0 are the hardness and fluence corresponding to the peak of the light curve, respectively. A similar empirical relation was found by Crider et al. ([23]) from a sample of 41 pulses, although they used the energy fluence instead of the photon fluence, which was linear rather than the exponential. Liang & Kargatis ([94]) proposed that the decay constant Φ_0 is mostly invariant among different pulses of the same burst: this was interpreted as the signature of a recursive event generating the burst rather than of a single catastrophic event. This conclusion was discussed by Crider et al. ([23]), extending the sample of pulses and questioning the possibility that this parameter be constant only by coincidence.

The other empirical relation describing the decay phase of a pulse is the Hardness Intensity Correlation (HIC) which, from the spectral analysis of a sample of 28 pulses, resulted to be:

$$E_{peak}(t) = E_{peak,0} \left[\frac{N(t)}{N_0}\right]^{\delta} \tag{2.4}$$

where δ is the correlation index and $N(t)$ is the photon flux (Kargatis et al. [76]). They interpreted this correlation as the signature of the saturated comptonization model (Liang [96]). As discussed in Ryde & Svensson [137] this model could account different spectral evidences, although some of its predictions are quite extreme (see chapt.6).

The combination of the HIC and HFC leads to the dependence of photon flux $N(t)$ and peak energy $E_{peak}(t)$ from time (Ryde & Svensson [137]):

$$N(t) = \frac{N_0}{(1 + t/\tau)} \tag{2.5}$$

$$E_{peak} = \frac{E_{peak,0}}{(1 + t/\tau)^{\delta}} \tag{2.6}$$

where τ and δ are free parameters.

These correlations (HIC and HFC) are strongly dependent on the parameters used to represent the hardness and the intensity, as recently pointed out by Borgonovo & Ryde ([11]). In fact, the integration of the spectrum over the detector bandpass to derive the intensity, can be influenced by the superposition of different spectral tails (at low energies, for instance) which are the residuals of the spectral evolution of previous pulses.

On the other hand Borgonovo & Ryde ([11]) propose to use the value of the νF_ν spectrum corresponding to the peak energy E_{peak} to indicate the intensity. They study a sample of 82 pulses, within 66 BATSE bursts, and find that in 57% of these the HIC is described by a power law:

$$\phi \propto E_{peak}^{\eta} \tag{2.7}$$

where ϕ is the intensity measure and the value of η, for single peaked bursts, is centered around 2 but with a wide dispersion. The same parameter seems to remain constant within multi-peaked bursts and this is an indication of a possible "memory" of the process (see below). In fig.2.4 and 2.5 are reported some examples of the HIC from Ryde & Petrosian ([138]). In fig.2.4 this relation is characterized by an index $\eta \sim 2$ whereas fig.2.5 reports a case of departure from this general value. The example reported in fig.2.5b and d are examples of the hard–to–soft evolution while fig.2.5c is an example of tracking morphology.

These findings have important implications for the emission model of GRBs: in fact if the internal shock model is based on the collision of different shells with different physical and geometrical parameters, it is unlikely that the same conditions are reproduced at every shock front but it is likely that the same stochastic distribution of physical parameters could be realized in different bursts. This implies that the expected dispersion in the HIC index could be seen in different bursts. On the other hand the internal shock model should explain the fact that in some multi–peaked bursts the correlation index is quite constant. This could be more easily explained by the single shell model in which the activation of different regions could give rise to the observed pulses with more or less the same HIC law. Furthermore, Borgonovo & Ryde ([11]) report a new evolutionary feature: a track-jump corresponding to a transition to successive pulses in multi-peaked bursts. This new evidence could be the result of the superposition of indistinguishable pulses.

The importance of the quantitative analysis of the HIC is that it could reveal the possible existence of a kind of "memory" among pulses: in fact if the peaks are the superposition of different emission episodes it could happen (in the case of "memory") that the second emission episode is influenced by the environmental modification induced by the previous emission episode, and this small scale relation among subsequent spikes can be reflected in some evolutionary morphology, like, for example, the presence of an hard to soft envelope. This is just a tentative idea which has not been investigated yet but which should have some testable predictions in the field of the spectral evolution analysis.

Low energy spectral component

The low energy component of GRB spectra is typically described by the portion of the spectrum below the peak energy and, in particular, by the spectral index α of the fitted

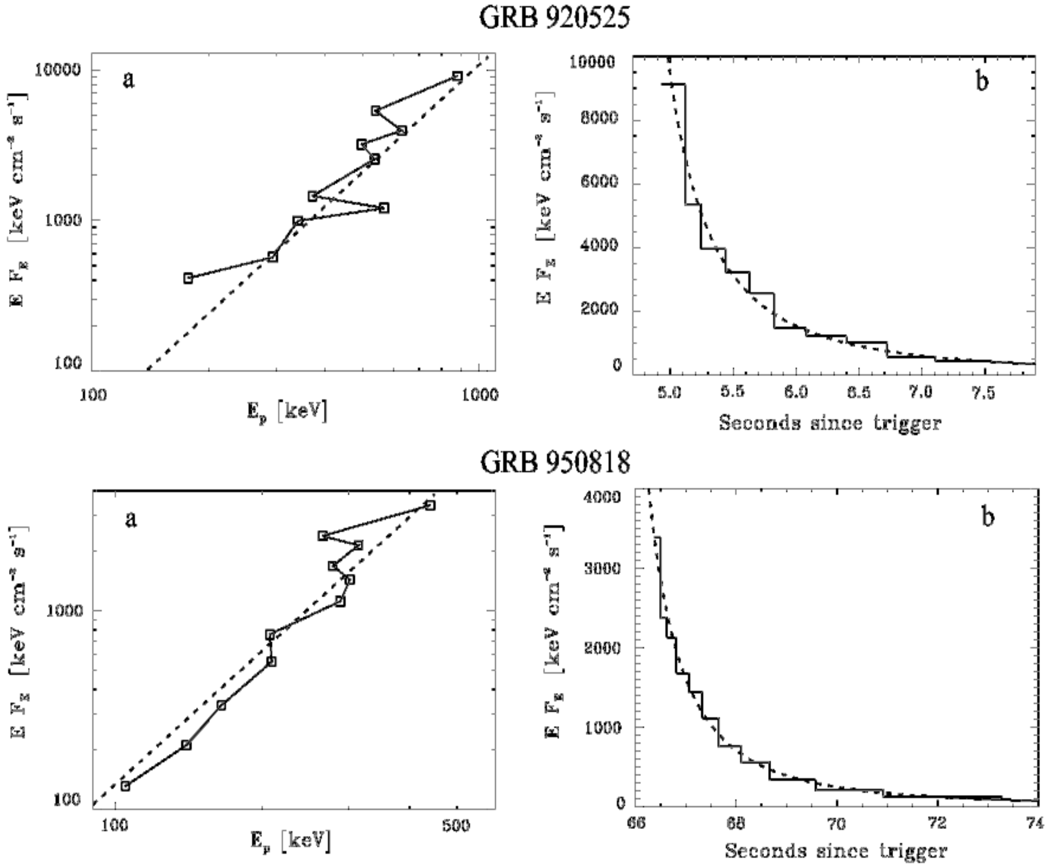

Figure 2.4: Examples of Hardness Intensity Correlation from Ryde & Petrosian (2002).Right panels (b) report the observed time evolution of the intensity (*solid histogram*) which is obtained assuming the HIC and the HFC relations (*dashed curves*). Panels (a) represent the HIC in log-log scale and the *dashed line* is the relation of eq. 1.8 with $\eta \sim 2$

power law. The distribution of this spectral parameter from the fits to the time resolved spectra of a large sample of bursts (from Preece et al. [130]) is reported in fig.2.6.

They found, from 5500 time resolved spectra, that α has a quite normal distribution with central value $\alpha = -1$. It is interesting to notice, also for the discussion of chap.5 and chap.6, that they have a quite large spread in the values of the low energy spectral index which extends far above the optically thin synchrotron model limit of -2/3 (see chapt.3). They suggest that this spread in the α distribution could be produced by the spectral evolution of the bursts.

It should be noticed that in this distribution (as in the others presented in the next sections from Preece et al. [130]) the possible dependence from the spectral model adopted to fit the spectra is not considered. In fact, they choose, as best model, the one fitting the time integrated spectrum: the fast spectral evolution of some bursts could determine an average spectrum with particular features (e.g. a smooth curvature

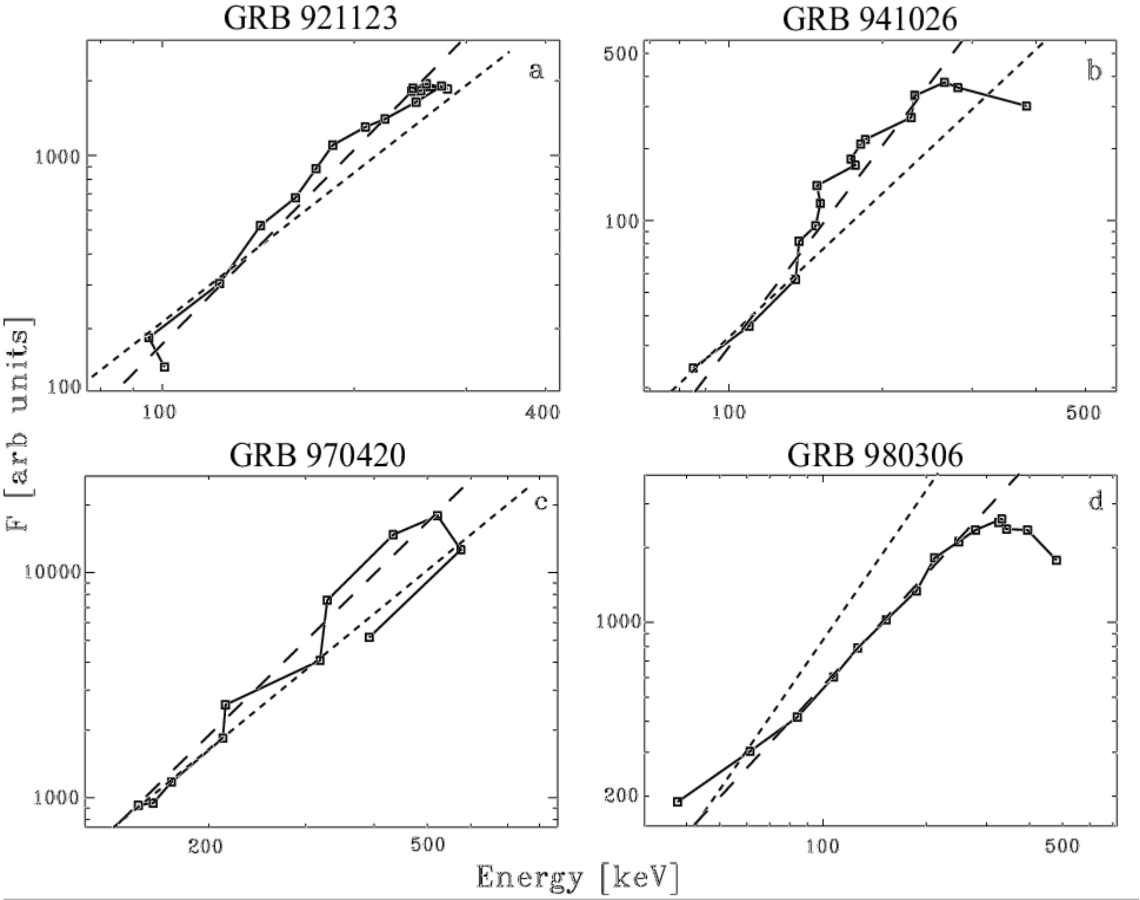

Figure 2.5: Examples of Hardness Intensity Correlation from Ryde & Petrosian (2002). Same as fig.2.4. The *long–dashed* lines are the fits to the observed HIC.

or an high energy power law tail) which result only from the superposition of many time resolved spectra but which are not necessarily present in the same time resolved spectra. This, coupled with the fact that the time resolved spectra, due to the lower S/N if compared to the time integrated, can be reasonably well fitted by different spectral models, should caution in interpreting the distribution of these spectral parameters.

In addition to this, in Preece spectral catalog, the spectral parameters of the time resolved spectra which result in unacceptable fits are set to the value obtained from the time resolved spectrum: this could lead to a biased interpretation of the spectral evolution because the time resolved spectrum can be different from the time integrated as shown in chap.5.

The temporal evolution of the low energy photon spectrum as represented by $\alpha(t)$ was considered an experimental evidence against those theoretical models, like the simplest synchrotron model (e.g. Katz 1994), which predict a fixed value for this spectral component. Crider et al. ([23]) found that the value of α, describing the low energy power law component of the time resolved spectra, evolves with time rather than remaining fixed

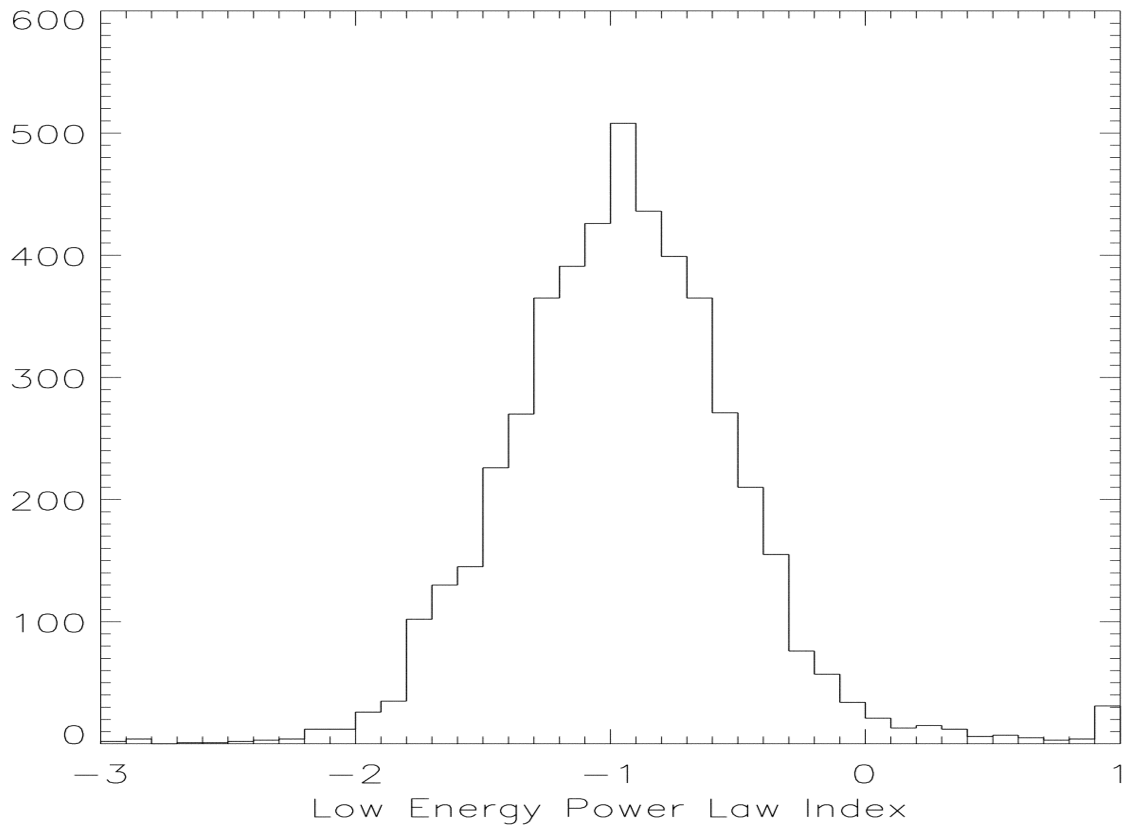

Figure 2.6: Low energy spectral index α distribution. From Preece et al. [130].

at the value of the time integrated spectrum in 58% of cases of their sample. They also observe a positive correlation between α and E_{peak} in a sample of 18 hard to soft and 12 tracking bursts at a high level of confidence (99.7% and 98% respectively). In the tracking cases, there is evidence that the value of α can be higher (harder spectrum) in the early burst phase. This could be another evidence of the existence of an evolutionary envelope, not only as represented by the break energy (Ford et al. [42]), but also by the low and high energy spectral components.

Some examples of the α evolution are reported in fig.2.7. GRB 911031 has an hard to soft spectral evolution described by its peak energy (*diamonds*) and the same behaviour characterizes the evolution of α (*crosses*). GRB 920525 is an example of tracking evolution which reproduces the flux change. GRB 931126 displays a mixed evolution, i.e. hard to soft and tracking on the first and second pulse, respectively.

High energy spectral component

The high energy spectral component can be characterized by a power law $\propto E^{\beta}$ with spectral index β, if the spectrum is represented by the BAND model. The distribution of

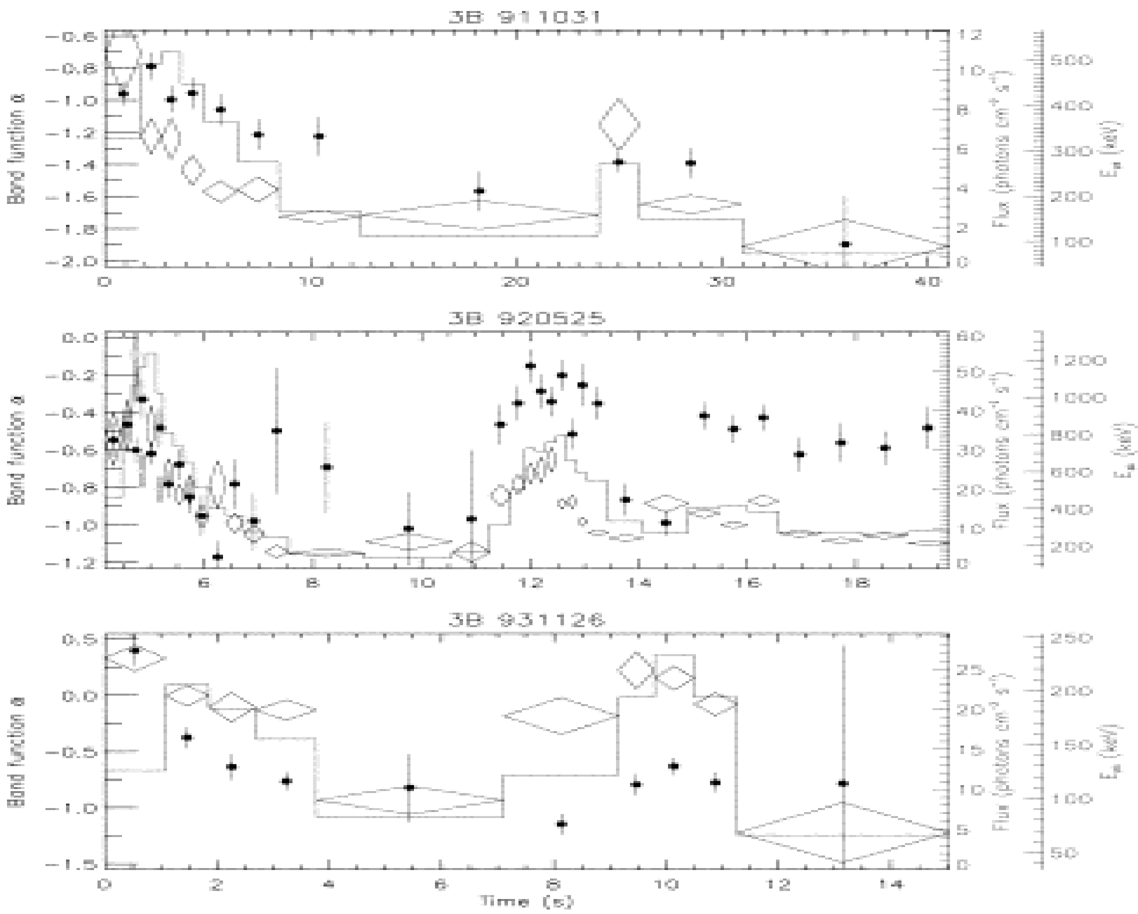

Figure 2.7: Examples of the evolution of the low energy spectral index α as reported by Crider et al. [21]. The peak energy E_{peak} (*diamonds*) and α (*crosses*) evolution are reported on the burst photon light curves.

β, as reported by Preece et al. ([130]), is centered around -2.25 although it has a broad dispersion as shown in fig.2.8.

A detailed analysis of the high energy spectral component in a sample of 126 bursts has been performed by Preece et al. ([129]). They fitted the BAND model to the time resolved spectra and applied statistical tests to verify the significance of their findings:

- β evolves with time rather than being constant in the 34% of their sample and the distribution of the average value of β is centered around -2.12;
- the excursion of this spectral parameter around its average value within most bursts is typically 0.4 which is small if compared with the typical variation of α and E_{peak};
- β evolves with time mainly (50 cases) with an hard to soft morphology and only 5 cases present a soft to hard β evolution.

The authors conclude that the evolution of the high energy spectral component is independent from the evolution of the other parts of the spectrum and it is small if